# Geometric Scaling of Tabular Igneous Intrusions: Implications for Emplacement and Growth

A.R. Cruden, K.J.W. McCaffrey and A.P. Bunger

**Abstract**

The horizontal ($L$) and vertical ($T$) dimensions of broadly tabular, sub-horizontal intrusions of mafic to felsic composition emplaced into shallow to mid-crustal levels of continental crust reveal two well-defined and continuous curves in log $L$ vs. log $T$ space. The data set spans six and five orders of magnitude in $L$ (1 m to 1000 km) and $T$ (10 cm to 10 km), respectively. Small tabular sheets and sills (mafic and felsic) define a straight line with a slope $\sim$ 0.5 at all horizontal length scales, similar to the known geometric scaling of mafic dikes, indicating that the $L/T$ ratio of these intrusions to increases with increasing $L$ (horizontal lengthening dominates over vertical thickening). Laccoliths, plutons, layered mafic intrusions and batholiths define an open, continuous S-shaped curve that bifurcates from the tabular sheets and sills curve at $L \sim$ 500 m towards higher $T$ values. For $L \sim$ 0.5 to 10 km the slope of this curve is $\sim$ 1.5, corresponding to laccoliths that are characterized by a decrease in $L/T$ ratio with increasing $L$ (vertical thickening dominates over horizontal lengthening). Between $L \sim$ 10 and 100 km the slope has a mean value $\sim$ 0.8, indicating that plutons and layered mafic intrusions have a tendency for horizontal lengthening over vertical thickening as $L$ increases. Batholiths

A.R. Cruden ($\boxtimes$)
School of Earth, Atmosphere and Environment,
Monash University, Melbourne, VIC 3800, Australia
e-mail: sandy.cruden@monash.edu

K.J.W. McCaffrey
Department of Earth Sciences, University of
Durham, Durham DH1 3LE, UK

A.P. Bunger
Department of Civil and Environmental Engineering,
University of Pittsburgh, Pittsburgh, PA 15261, USA

A.P. Bunger
Department of Chemical and Petroleum Engineering,
University of Pittsburgh, Pittsburgh, PA 15261, USA

and very large layered mafic intrusions with $L > 100$ km lie on a slope $\sim 0$ with a threshold thickness $\sim 10$ km. The continuous nature of the dimensional data over such a wide range of length scales reflects a spectrum of igneous emplacement processes repeated in space and time. We discuss how thresholds and transitions in this spectrum, defined by bifurcations between the curves (e.g., between sill and laccolith emplacement) and changes in slope, largely reflect depth- and time-dependent changes in emplacement mechanisms rather than factors such as magma viscosity, composition and temperature.

## 1 Introduction

Dimensional scaling data of tabular igneous intrusions has been employed in several contexts to progress understanding of emplacement mechanisms. For example, the dimensional scaling of plutons and laccoliths has been used qualitatively to contrast their emplacement mechanisms, namely the relative roles of horizontal lengthening versus vertical thickening, the relative contributions of roof lifting in the shallow crust (laccoliths) versus floor subsidence in the middle to lower crust (plutons) and to discuss whether they grow by a single or multiple step process (McCaffrey and Petford 1997; Cruden and McCaffrey 2001). Dimensional scaling data from mafic dikes has been employed to determine dike initiation conditions and magma driving pressures (Babiker and Gudmundsson 2004; Gudmundsson 2011a, b) and to differentiate between propagation regimes predicted by Linear Elastic Fracture Mechanics (LEFM) (Delaney and Pollard 1981; Olson 2003; Schultz et al. 2008a; see review of Rivalta et al. 2015). Similarly, Bunger and Cruden (2011a) developed a combined LEFM-fluid mechanics model for the emplacement of sills and laccoliths that attempts to explain the different power-law scaling relationships of both types of intrusion as well as several leading-order geometric features, such as the flat tops and steep sides of laccoliths. Abdelmalak et al. (2012) and Galland and Scheibert (2013) have shown experimentally and theoretically that interpretation and prediction of

surface deformation related to shallow magma emplacement is critically dependent on understanding natural intrusion shapes and morphologies.

In this chapter we present the most recent compilation of available dimensional data from tabular igneous intrusions. The data set spans six orders of magnitude in the horizontal dimension and five orders of magnitude in the vertical dimension. We focus on the implications of the data for understanding emplacement and growth mechanisms of dykes, sills and laccoliths, and highlight gaps in understanding igneous intrusion processes as avenues for future research.

## 2 Geometric Scaling Analysis

It has been shown previously that there is a power-law scaling relationship between the vertical thickness, $T$, and horizontal length, $L$, of laccoliths and plutons described by

$$T = bL^a, \qquad (1)$$

where $a$ is the power-law exponent and $b$ is a constant (McCaffrey and Petford 1997; Cruden and McCaffrey 2001; Cruden 2006). Dimensional measurements of both mafic dikes, in which case $T$ is the horizontal width, and sills are also consistent with power-law scaling relationships (Olson 2003; Babiker and Gudmundsson 2004; Schultz et al. 2008a; Klimczak et al. 2010; Bunger and Cruden 2011a). Alternatively, if sufficient three-dimensional information is

available a power-law relationship between $T$ and intrusion volume, $V$, can also be proposed:

$$T = dV^c \qquad (2)$$

where $c$ is the power-law exponent and $d$ is a constant.

For the purpose of this analysis, for approximately horizontal intrusions we define $L$ as the equivalent diameter of a circle given by measurements of either the major and minor axes of elliptical bodies or their areas, and $T$ as the mean vertical thickness value where data are sufficient.

For dykes, $L$ is the horizontal trace and $T$ is the horizontal width, both in map view. To estimate $V$, we assume that horizontal tabular intrusions are disk shaped such that $V = \pi T(L/2)^2$. This is a reasonable first-order assumption for sills, minor sheets, meso-scale intrusions and laccoliths. However, it is known that plutons and layered intrusions are characterised by end-member wedge- and disk-shaped morphologies (Vigneresse 1995; Cruden 2006) so $V$ will be overestimated for the former type. We do not attempt to estimate $V$ for dykes as the vertical height is rarely constrained. However, we note that recent

**Table 1** Dimensional data and power law scaling parameters of tabular intrusions

| | $N$ | $L$ (km) | $T$ (km) | $L/T$ | $a$ | $b$ (m) | References |
|---|---|---|---|---|---|---|---|
| Batholiths | 4 | 95–600 | 3–15 | 20–90 | – | – | Cruden (2006) |
| Plutons | 61 | 3.5–86 | 1–10 | 1.5–17 | 0.81 ± 0.12[a] | 1.08 ± 1.38[a] | Cruden (2006), McCaffrey and Petford (1997), Cruden and McCaffrey (2001) |
| Layered Mafic intrusions | 8 | 8–550 | 3–13 | 2.3–68.7 | – | – | |
| Laccoliths | 131 | 0.3–80 | 0.03–3 | 2–50 | 0.92 ± 0.11 | 0.12 ± 0.02 | McCaffrey and Petford (1997), Corry (1988) |
| Henry Mtns | 38 | 0.8–7.2 | 0.03–2.5 | 1.8–25.8 | 1.77 ± 0.36 | 0.07 ± 0.02 | Corry (1988) |
| La Sal Mtns | 10 | 0.8–5.6 | 0.2–1.0 | 3.8–12.3 | 1.52 ± 0.39 | 0.12 ± 0.04 | Corry (1988) |
| Sleeping Ute Mtns | 14 | 0.8–3.6 | 0.06–0.76 | 2.6–17.8 | 1.83 ± 0.77 | 0.09 ± 0.03 | Corry (1988) |
| Abajo Mtns | 32 | 0.3-6.4 | 0.1–0.78 | 1.9–13.3 | 1.06 ± 0.20 | 0.21 ± 0.02 | Corry (1988) |
| Elba Island | 9 | 1.6–10 | 0.05–0.7 | 11.8–33.3 | 1.41 ± 0.17 | 0.03 ± 0.01 | Rocchi et al. (2002) |
| Average for groups | | | | | 1.52 ± 0.31[b] | 0.02 ± 0.07[b] | |
| Horizontal Sheet Intrusions | 68 | 0.001-450 | 0.0001–0.6 | 1.9–2400 | 0.57 ± 0.02 | 0.4 ± 0.22 | |
| Mafic sills (L > 1 km) | 31 | 1–450 | 0.01–0.6 | 10–2400 | 0.85 ± 0.1 | 0.01 ± 0.02 | Bunger and Cruden (2011a) |
| Mesoscale intrusions | 13 | 0.14–1.6 | 0.0005–0.025 | 37–290 | 0.49 ± 0.13 | 0.47 ± 0.33 | Corazzato and Groppelli (2004) |
| Minor Intrusions (Skye) | 17 | 0.001–0.004 | 0.0001–0.0005 | 1.9–9.2 | 0.91 ± 0.25 | 0.27 ± 0.04 | Walker (1993) |

[a]RMA regression for plutons and layered mafic intrusions, excluding the Bushveld complex
[b]Average of $a$ or $b$ values; error is given as 1 standard deviation

analytical work suggests that for swarms of blade-shaped dykes their height scales approximately to their horizontal spacing (Bunger et al. 2013).

Because $T$ and $L$ (and $V$) are dependant variables, analysis of individual sets of intrusion data, subdivided by intrusion type and geographical location were carried out by Reduced Major Axis regression (RMA) (McCaffrey and Petford 1997; Smith 2009). This method is preferred over the Ordinary Least Squares method because there is no a priori reason why the measurement errors in $L$ (and $V$) and $T$ should be asymmetrically distributed. Mean values of the power-law exponent, $a$, and ranges of values of the intercept, $b$, for groups and sub groups of intrusions are summarized in Table 1.

## 3 General Characteristics and Scaling of Tabular Intrusion

Log thickness, $T$, and log length, $L$, data from >320 sub-horizontal tabular intrusions and $\sim 90$ sub-vertical mafic dikes are plotted in Fig. 1a. For comparison, log $T$ is plotted against log $V$ in Fig. 1b. More than 99% of the data are derived from peer-reviewed literature sources and comprise measurements based on field observations (maps, cross sections, exposures in high relief areas, boreholes) and geophysical surveys (forward modelling of 2D and 3D gravity data and interpretation and analysis of seismic reflection data). As noted in previous work (e.g., Cruden 2006), no obvious difference is found between intrusion dimensions determined by field and geophysical methods, except for very large intrusions with $L > 50$ km, which are too large to provide field-based means for thickness estimation.

All classes of intrusion analysed here display well-defined power law scaling relationships between $T$ and $L$ (Fig. 1a; Table 1). In general, the exponent, $a$, differentiates between growth behaviour in which the aspect ratio $L/T$ is increasing ($a < 1$, "lateral spreading") and decreasing ($a > 1$, "uplifting"). This is well illustrated in the log $L/T$ versus log $L$ de-correlation plot (Fig. 2). For laccoliths, the

growth regime favours uplifting with $a > 1$. Indeed, when applied to individual provinces, $a$ has been observed to be as large as 1.5 (Rocchi et al. 2002). In contrast, plutons, large mafic sills, mafic dykes and minor and mesoscale sheets favour lateral spreading with $a < 1$.

A pronounced feature of the log $T$ versus log $L$ data plot is a bifurcation between the array for minor sheets, mesoscale sheets, sills and dykes, which fall along a fit line with $a \sim 0.5$, and the array for laccoliths ($a \sim 1.5$), plutons ($a \sim 0.8$), layered mafic intrusions and batholiths ($a$ approaches 0) (Fig. 1a). The bifurcation occurs where $L \sim 500–1000$ m and $T \sim 10–30$ m. The log $T$ versus log $V$ plot also shows a similar bifurcation between the data arrays, occurring where $V \sim 1 \times 10^7 – 1 \times 10^8$ m$^3$ (0.01–0.1 km$^3$) and between slopes of $c \sim 0.3$ for sills and $c \sim 0.4$ for laccoliths (Fig. 1b). Both plots also highlight several important differences between intrusion types. For example, sills and laccoliths share a similar range of thickness but sills have approximately one order of magnitude greater length and two orders of magnitude greater volume. Similarly, although there is overlap between the lengths of the largest mafic sills and those of batholiths and very large layered mafic intrusions (Fig. 1a), the latter two classes of intrusion are $\sim 1.5$ orders of magnitude thicker and have volumes one to two orders of magnitude greater than the largest sills (Fig. 1b). The change in slope between the laccolith array and the plutons and layered mafic intrusions array is also much less pronounced, if not absent, in the log $T$ versus log $V$ plot, with all three classes of intrusions sharing an RMA slope of $c \sim 0.38$.

The first-order geometric characteristics and scaling relationships for individual classes of intrusion are discussed in more detail below.

### 3.1 Mafic Dykes

Mafic dykes are vertical to sub-vertical tabular intrusions that transport mafic magma both vertically and laterally in the crust. They occur over a wide range of scales from crustal-scale giant
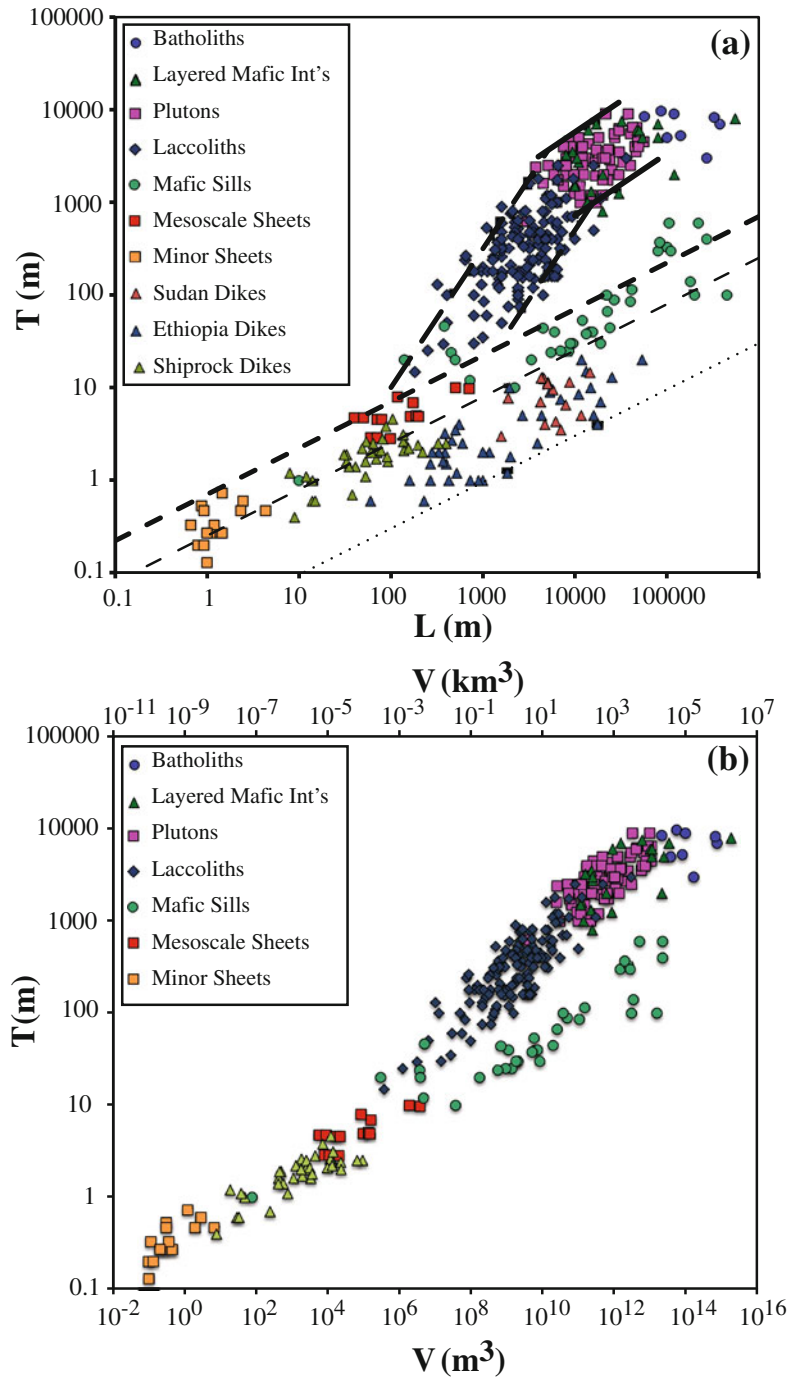
radiating and linear swarms that transport enormous volumes of mantle-derived magma associated with Large Igneous Province events (e.g., Ernst et al. 2005) to kilometer to decameter-scale individual dykes and dyke swarms associated with moving magma from mid-crustal to shallow magma chambers toward the surface to feed volcanic eruptions (e.g., Geshi et al. 2010). Dykes are also integral components of crustal-scale magma transport networks,
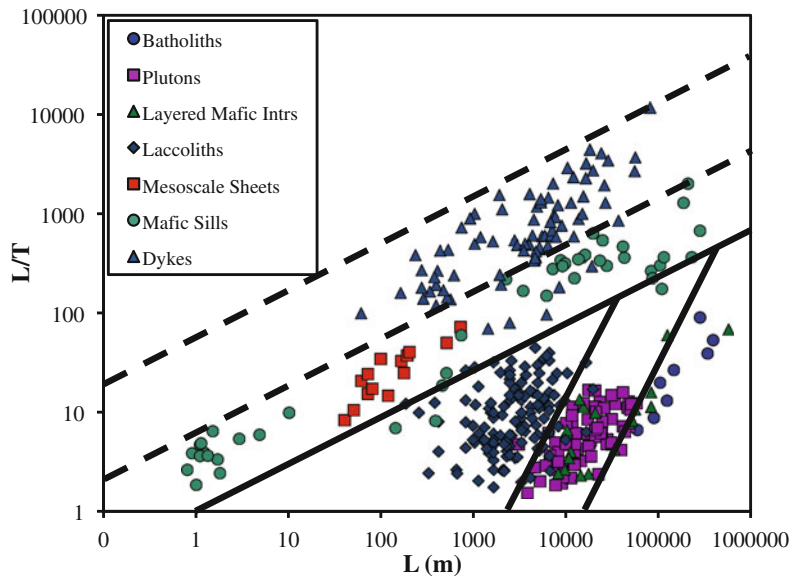
connecting mantle reservoirs to sills and layered intrusions and eventually the surface (Marsh 2004; Barnes et al. 2016). Although the first-order tabular or blade-shaped geometry of dykes is simple, individual dykes and dyke swarms can show considerable structural complexity owing to their mode of propagation and interactions with country rock structure and other dykes. Examples of such complexity include the propagation of en echelon dykes and their eventual bridging and linkage (broken bridges) (Nicholson and Pollard 1985; Schofield et al. 2012), bifurcation, deviation and arrest due to intersection with pre-existing fractures and mechanical barriers (Gudmundsson 2011a, b; Rivalta et al. 2015). Such complexity is not captured by the scaling data.

The mafic dyke data sets used here come from observations and measurements in the USA (Ship Rock; Delaney and Pollard 1981), Ethiopia (Schultz et al. 2008b) and Sudan (Babiker and Gudmundsson 2004). The data span a horizontal length range from $L \sim 10$ m to 50 km and thicknesses $T \sim 0.5$–20 m. Clearly, this data set is limited in that it misses out measurements from giant radiating and linear dyke swarms in which individual dykes can be traced for 100–1000 s of kilometers with widths in the 10 s of meters (e.g., Halls and Fahrig 1987). Unfortunately, reliable

measurements from such settings are hard to come by as the true lateral extent of very long dykes is hampered by poor geological preservation and thickness data is limited, often relying on poorly constrained estimates from aeromagnetic data.

Although the focus here is on sub-horizontal tabular intrusions, mafic dikes are included for comparison and because LEFM is also proposed to control their emplacement (Olson 2003; Gudmundsson 2011a). Consistent with previous analyses (Schultz et al. 2008a, b), the mafic dikes analysed here are characterized by power-law slopes with $a \sim 0.5$ and the combined dataset can be bounded by lines with $b = 0.03$–0.25 (Fig. 1a). Mafic dikes share a common power-law slope with mafic sills and mesoscale and minor sheets but they are systematically thinner, with a greater *L/T* ratio for any given length (Fig. 2).

## 3.2 Sills and Sub-horizontal Sheets

Sills and sub-horizontal sheets are generally thought to have simple disk or penny shapes with uniform thickness and parallel upper and lower contacts that are concordant to the enveloping strata over most of their area, and tapered margins (Fig. 3). Unlike laccoliths (see below), sills
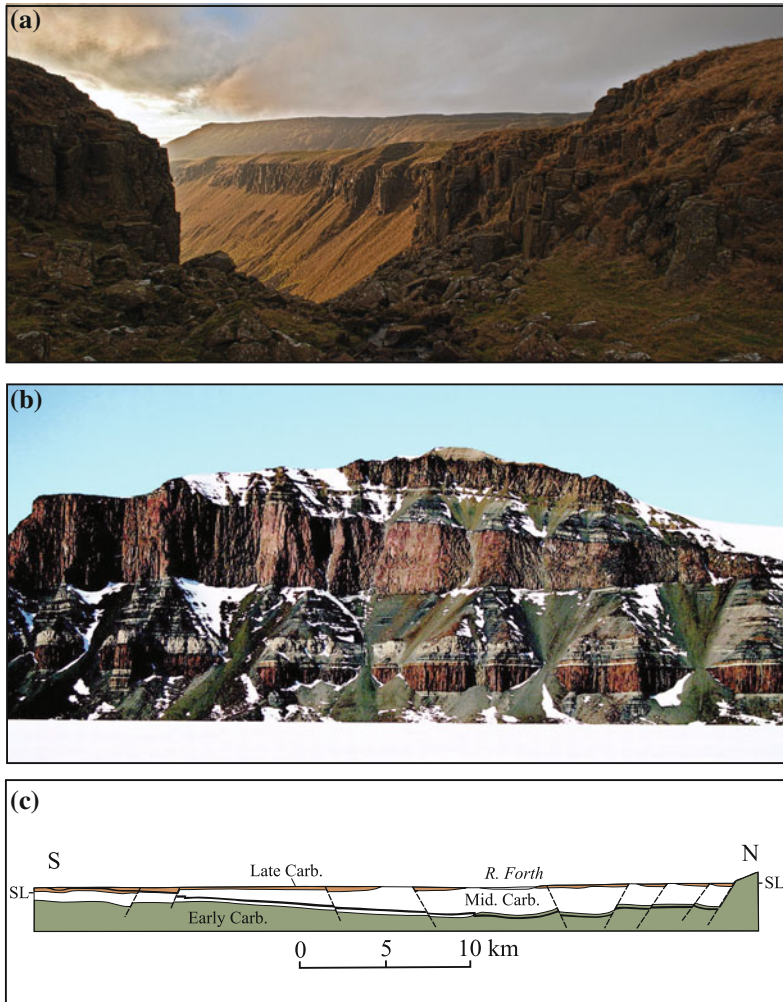
**Fig. 3** **a** Valley exposure of the Cretaceous Whin Sill showing uniform thickness and parallelism with country rock strata, High Cup Nick, Cumbria UK (photograph courtesy of M. Lishman). Sill is ∼30 m thick. **b** Vertical exposure of Jurassic sills at Coalseam Cliff, Theron Mountains, Antarctica [courtesy of Hutton (2009), Fig. 14]. The Scarp Capping Sill is observed in the center of the cliff, where it clearly tapers to the south (*right*) from a regional thickness of 200 to <70 m. Cliff is 700 m high. **c** North-south cross section of the Permian Midland Valley sill, Scotland (after Francis 1982). The sill (*black*) intrudes early Carboniferous volcanics in the north and transgresses upward to the south through middle and upper Carboniferous sediments, respectively. The sill has a maximum thickness of 150 m at its deepest point below the River Forth, decreasing to <10 m to the south

display little or no evidence for up bending of overlying strata. However, like dykes their simple first-order geometry is often more complex in detail. For example, some sills exhibit concave-up, saucer-shaped geometries, which in cross sections with no vertical exaggeration have dihedral angles of >160° (Fig. 3c) (e.g., Malthe-Sørenssen et al. 2004; Galland et al. 2009; Planke et al. this volume). Some sills exhibit stair-stepping geometries in cross section that are regionally transgressive to stratigraphy (Fig. 3) (e.g., Bradley 1965; Thomson and Schofield 2008; Bédard et al. 2012; Muirhead et al. 2012; Magee et al. 2016; Walker 2016). Three-dimensional seismic surveys of sedimentary basins have revealed sills with complex

lobate and elongate morphologies (e.g., Thomson 2007; Thomson and Hutton 2004) that are similar to the margins of lava flows and to lava channels, respectively. As with dykes, this complexity is not reflected in the scaling data, nor do most analytical and numerical models of emplacement explain it. However, it should be noted that three-dimensional analogue experiments have successfully simulated saucer-shaped geometries and complex lobate margin structure (Hansen and Cartwright 2006; Miles and Cartwright 2010; Galland et al. this volume).

The sills and sheets data array comprises sub-horizontal, meter-scale minor mafic sheets (Skye; Walker 1993), mesoscale ($L \sim 40$–700 m) intermediate sheets (Montecampione; Corazzato and Groppelli 2004) and mafic sills ranging from $L \sim 10$ m to 450 km. The minor/mesoscale sheets and mafic sills data array is represented predominantly by fine grained igneous rocks with low silica contents (i.e., basaltic $\gg$ trachytic and phonolitic compositions). The intrusions analysed here were mostly emplaced into layered sedimentary host rocks at shallow depths (<100 to 3000 m) (e.g., Bradley 1965; Mudge 1968; Francis 1982; Leaman 1975). However, it is known from seismic reflection profiles and tilted crustal sections that sills and sheets occur at deeper levels in the crust, including the crust-mantle boundary (Quick et al. 1994; McQuarrie and Rogers 1998). Unfortunately, lack of outcrop continuity and insufficient spatial resolution of seismic reflection data make it difficult to acquire scaling data for this class of intrusion at depths more than a few kilometres.

Although there is a reasonable amount of data (36) from mafic sills with $L > 1000$ m in the literature, there is limited geometrical information for smaller intermediate and mafic sheets. Nevertheless, the individual mafic sills and mesoscale/minor sheets data are characterized by power-law slopes with $a \sim 0.5$ and the combined dataset can be bounded by lines with $b = 0.25$–0.7 (Fig. 1a). Several very large mafic sills with $L > 80$ km lie above these bounds and may represent multi-pulse, stacked intrusions (see below). A subset of the smaller mafic sills also lies above this line, suggesting that they

would be better classified as laccoliths. The power-law scaling for the complete data set indicates that the $L/T$ ratio of sills and sub-horizontal sheets increases systematically from as low as $\sim 2$ for $L \sim 1$ m to as high as $\sim 2000$ for $L \sim 20{,}000$ m (Fig. 2).

## 3.3 Laccoliths

Laccoliths usually have flat floors, steep sides and slightly arched roofs (Fig. 4) and are generally considered to be emplaced at depths that rarely exceed 3000 m (e.g., Pollard and Johnson 1973; Corry 1988). They are typically made up of fine-grained to hypabyssal-textured rocks with basaltic to rhyolitic compositions (Corry 1988), occur in all tectonic environments throughout the geological record, and are commonly, but not always, associated with volcanism. Deeper (e.g., de Saint Blanquat et al. 2001) and or larger (e.g., Michel et al. 2008) gabbroic to granitic laccoliths are characterized by coarse-grained plutonic textures, and some of these are also emplaced into crystalline country rocks (Fig. 4c) (e.g., Cruden 2008; Friese et al. 2012).

The type region for laccoliths are the Tertiary igneous provinces of the western interior United States (Corry 1988), including the Henry Mountains where the laccolith concept was first formulated by Gilbert (1877) and carefully documented by Hunt et al. (1953), Johnson and Pollard (1972), and Jackson and Pollard (1988), among others. The majority, but not all (e.g., Friese et al. 2012), of the laccoliths intrude layered sedimentary rocks, and based on the bell-jar profile of deflected strata from the sides over the roof (e.g., Fig. 4a; Gudmundsson et al. this volume), they are inferred to grow by upward bending of their wall rocks during vertical inflation of magma after initial emplacement of a bedding parallel sill (Pollard and Johnson 1973). Field and geochronological studies indicate that laccolith growth commonly occurs by multiple injections of sheets over time-scales ranging from 100 years to 100 ka (Jackson and Pollard 1988; de Saint Blanquat et al. 2006, 2011; Leuthold et al. 2012).
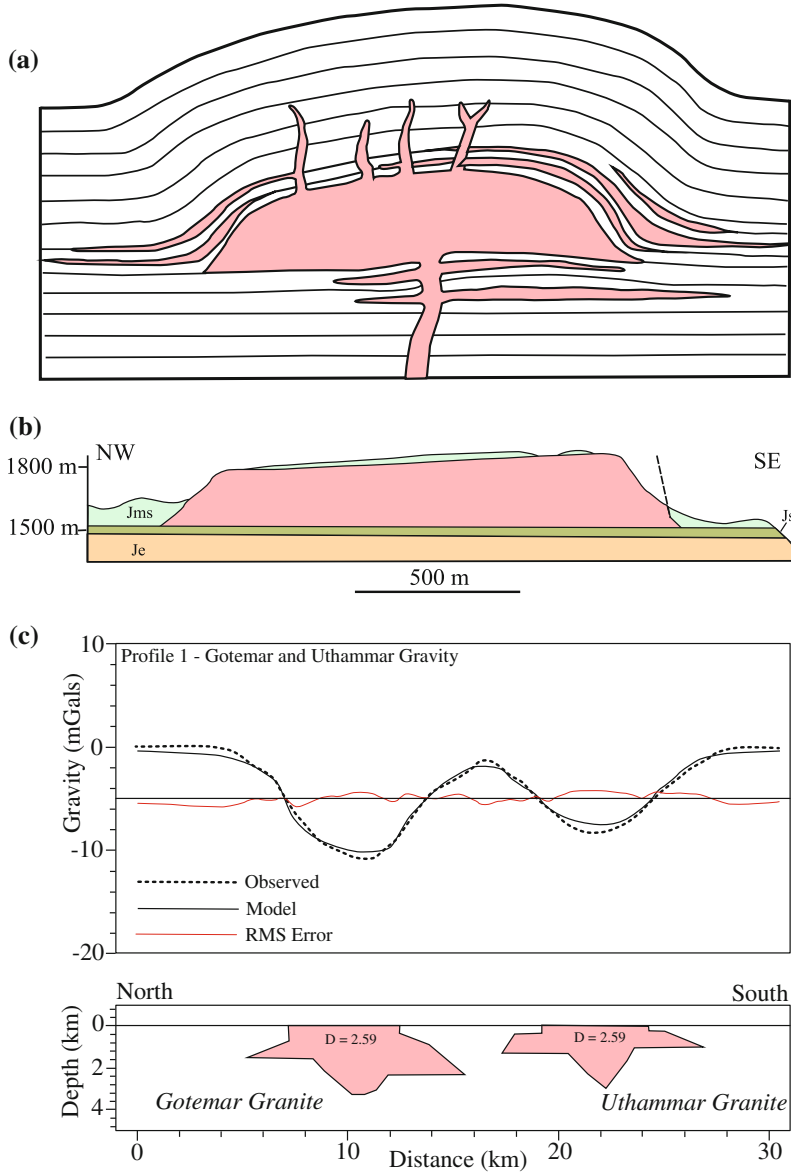
**Fig. 4** **a** G.K. Gilbert's conceptual cross section of laccoliths in the Henry Mountains, Utah (after Gilbert 1877; Corry 1988). Laccolith is *pink*, and *curved lines* represent traces of bedding in wall rock strata. **b** Cross section of the Oligocene Black Mesa laccolith (or bysmalith; Corry 1988), Henry Mountains, Utah (after de Saint Blanquat et al. 2006). Pink is diorite; Jms is Jurassic Morrison formation (sandstone); Js is Jurassic Summerville formation (shale); Je is Jurassic Entrada formation (sandstone). Note flat-topped profile of laccolith and faulted southeast margin. **c** Residual gravity anomaly profiles (*above*) over the Mesoproterozoic Götemar and Uthammar granites in south east Sweden and corresponding 2.5 D forward gravity models (*below*), constrained by borehole data. Both granites intrude crystalline rocks but have laccolithic forms. *Dotted curve* = gravity data, *solid black curve* = forward gravity model, *red curve* = RMS error, granite bodies in forward model are *pink*. After Cruden (2008; see also Friese et al. 2012)

Like dykes and sills, laccoliths are known to deviate from their ideal circular, bell-jar shape, forming intrusions with a variety of complexities that are not captured in the geometric scaling data. For example, some laccoliths are distinctly asymmetric in cross section bounded by a steep

fault on one margin and a tapered contact on the other (a.k.a., bysmalith; Fig. 4b) (e.g., de Saint Blanquat et al. 2006). Other laccoliths, such as the Maiden Creek and Trachyte Mesa, Utah, have tube and finger like morphologies and some laccolith margins have been shown to have lobe-shaped contact relationships in detail (Johnson and Pollard 1973; Horsman et al. 2010). However, recent work indicates that these examples may form as stacked saucer-shaped sheets rather than lobate fingers (Wilson et al. 2016). Stacked systems of tabular intrusions (e.g., Rocchi et al. 2002; Westerman et al. this volume) have also been referred to as Christmas-tree laccoliths (Corry 1988).

Most of the laccolith data analysed here are derived from a global database compiled by Corry (1988), updated, checked and censored to remove spurious and incorrect information. RMA analysis of the original laccolith dataset found a poorly determined power-law with $a \sim 0.88$ (McCaffrey and Petford 1997). Rocchi et al. (2002) subsequently analyzed laccoliths from the Island of Elba, Italy and found a robust power-law scaling relationship with $a \sim 1.5$. We have determined similar slopes for the individual major laccolith groups in the western USA (Corry 1988) and reassessment of the complete data set, including a handful of intrusions classified earlier as mafic sills (Fig. 1a), indicates that it can be bounded by lines with slopes of $a \sim 1.5$ and $b = 0.0005–0.01$ (Table 1). A key feature of the scaling data is that laccoliths are characterized by $a > 1$ so that they thicken faster than they lengthen; this leads to a general decrease in $L/T$ ratios from $\sim 30$ to $\sim 3$ between $L \sim 500$ and $\sim 8000$ m (Fig. 2), which is opposite to the trend displayed by sills and sub-horizontal sheets.

## 3.4 Plutons, Layered Intrusions and Batholiths

For the purpose of this analysis, plutons are coarse-grained felsic to intermediate intrusive bodies with circular, elliptical to irregular outer margins in map view that are emplaced in the upper to lower crust. Layered mafic intrusions have a similar geometry and range of emplacement depths but are made up of coarse-grained mafic and ultramafic rocks that often display distinct compositional layering at a variety of scales. Both plutons and layered mafic intrusions typically comprise more than one compositional phase or pulse and they can show simple (i.e., zoned) or complex internal structure. Batholiths are large composite intrusive masses that are made up of multiple plutons and, in some cases, layered mafic intrusions. Determination of the vertical dimensions of plutons, layered intrusions and batholiths relies on the use of geophysical techniques (gravity, magnetic, seismic reflection/refraction surveys), direct measurement in tilted crustal sections or regions with deep erosional dissection, or analysis of structural patterns (see Cruden 2006 and references therein). The floor and roof of the intrusion are commonly observed in cases where direct measurement can be made, whereas geophysical data typically only provides information on thickness from a sub-roof erosion level to the intrusion floor. Recent field and geochronological studies of plutons indicate that the majority are constructed by multiple pulses over timeframes ranging from ca. 0.1 to 6 Ma (Coleman et al. 2004; Miller et al. 2007; Michel et al. 2008; Schaltegger et al. 2009; de Saint Blanquat et al. 2011; Leuthold et al. 2012). Due to their composite nature, batholiths are constructed over 10 s of Ma.

The pluton data array ranges from 1000 to 9000 m in thickness and 3.7 to 54 km in length (Fig. 1a, Table 1). There is some overlap between the laccolith and pluton fields, which reflects some ambiguity in classifying intrusions in the $L = 4–10$ km size range. Layered mafic intrusions with $L < 80$ km are not distinguishable from plutons in terms of dimensions. We therefore treat both classes of intrusion together in the following analysis and discussion. Plutons and layered mafic intrusions are characterised by a power law scaling with $a = 0.81$ and the combined data set can be bounded by curves

with $b = 0.37$ and 3.13 (Fig. 1a). The $a < 1$ power law for these intrusions indicates a return to a geometric scaling in which lengthening dominates over thickening and a general increase in $L/T$ ratio from $\sim 5$ for smaller plutons to $\sim 10$ for the largest (Fig. 2). The transition from laccoliths to plutons can be described as a gradual change in scaling from $a > 1$ to $a < 1$ and therefore from a thickening- to a lengthening-dominated growth regime.

Batholiths and layered mafic intrusions with $L > 80$ km plot at the top right of the scaling diagram (Fig. 1a), ranging in thickness from $T = 2000–9700$ m and length from $L = 57–550$ km. Unlike the smaller classes of intrusion, there is no obvious dependence between thickness and length for batholiths and large layered mafic intrusions. Instead there appears to be a thickness threshold of $\sim 10$ km, corresponding to one third to one quarter the thickness of continental crust. The transition from plutons and small layered intrusions to batholiths and large layered mafic intrusions can be described as a change from a lengthening dominated growth regime with a <1 to a constant thickness regime.

## 4 Relationships Between Emplacement Mechanisms, Depth and Scaling Relationships

Although the dimensional data clearly separate different classes of intrusions in terms of size, shape (Fig. 1a), volume (Fig. 1b), aspect ratios and empirical $L$-$T$ scaling relationships (Fig. 2; Table 1), they do not capture information on depths of emplacement, $H$, compositions and timescales.

Following the material reviewed above, there is a general tendency for intrusions in the laccolith-plutons-layered mafic intrusions array to become deeper as $L$, $T$ and $V$ increase, although there is currently insufficient information that couples geometric data with emplacement depth to assess this rigorously. There is also a general tendency for larger intrusions to take longer to grow, which is a consequence of their greater volume and a limited range of likely magma

fluxes (e.g., Petford et al. 2000; Cruden 2006; de Saint Blanquat et al. 2011; Menand et al. 2015). Within the same data array there does not appear to be a major compositional control on geometry and scaling. Hence laccoliths are emplaced at shallower depths over shorter timescales than plutons and layered mafic intrusions but composition is not a differentiating factor.

Intrusions in the minor/mesoscale sheets and sills array vary in composition from basalt to trachyte and they are all emplaced at depths shallower than $\sim 3$ km. Hence, neither emplacement depth nor magma composition are likely to be differentiating factors controlling the power law scaling of these data. However, as sub-horizontal sheets and sills increase in size and volume the ratio between $L$ and the emplacement depth, $H$, will increase. This implies that small sheets with L ≪ H will propagate in a regime under which the dynamics of emplacement does not involve interaction with Earth's free surface (known in mechanics as the thick sheet approximation). Conversely, large sheets and sills with L ≫ H will be emplaced under conditions where intrusion growth is strongly coupled to the deformable free surface (known in mechanics as the thin sheet approximation). The transition between these two regimes will occur when $L \sim H$, which for our data set roughly corresponds to the bifurcation between the sheets and sills array and the laccoliths array at $L \sim 1000$ m. However, since laccoliths and sills share similar ranges of $T$ and are emplaced at comparable depths, the bifurcation cannot be related to the $L$-$H$ transition alone, as discussed below.

Whether the growth of tabular intrusions involves interaction with Earth's free surface ($L \gg H$) or not ($L \ll H$) defines two first-order emplacement regimes that will be used as the framework for the discussion below. However, it should be noted that this framework cannot apply to deeper plutons and layered mafic intrusions, which generally satisfy the condition $L > H$ but rarely show evidence for emplacement involving roof uplift and interaction with Earth's surface (e.g., Cruden 2006 and references therein). Vertical movement of country rocks is likely

involved in making space for these types of intrusions (e.g., Clough et al. 1909; Myers 1975; Paterson et al. 1996) but this process most likely involves displacements of interfaces below the level of emplacement (Brown and McClelland; Cruden 1998; Grocott et al. 2009).

## 4.1 Intrusions that Do not Interact with Earth's Surface

The minor/mesoscale sheets and smaller sills in the data array are generally emplaced under conditions where $L \ll H$, and therefore they are unlikely to interact with the surface during emplacement. Dykes can also be considered as intrusions that do not interact with the surface during their propagation and growth; hence they are included in the analysis below (Fig. 5). Under conditions where the magma pressure is spatially uniform and the growth of the intrusion is implied by $K_I = K_{Ic}$, where $K_I$ is the mode I stress intensity factor and $K_{Ic}$ is the mode I fracture toughness of the rock, LEFM predicts (e.g. Olson 2003):

$$T = \frac{K_{Ic}(1 - v^2)\sqrt{8}}{E\sqrt{\pi}}\sqrt{L}, \qquad (3)$$

where $E$ is Young's modulus and $v$ is Poisson's ratio. The $a \sim 0.5$ exponent of the $L$-$T$ scaling for mafic dykes (Delaney and Pollard 1981; Olson 2003; Schultz et al. 2008a, b) and minor/mesoscale sheets and smaller sills (Fig. 5) is therefore consistent with this LEFM prediction. However, as noted in previous studies, $K_{Ic}$ values 10–1000 times laboratory values are required to fit the different data sets (Delaney and Pollard 1981; Olson 2003; Schultz et al. 2008a; Cruden et al. 2009). For example, best fit curves that bracket the dyke, sheet and sill data in Fig. 5 are computed for values $E = 100$ GPa, $v = 0.3$ and $K_{Ic} = 300$–$3000$ MPa m$^{1/2}$ whereas typical laboratory rock toughness values range from 0.5 to 2 MPa m$^{1/2}$. The relationship between these bounding curves and the individual data sets also indicate that dykes require systematically lower effective fracture toughness values than sheets and sills, which as noted above tend to be also systematically thicker than dykes for any given
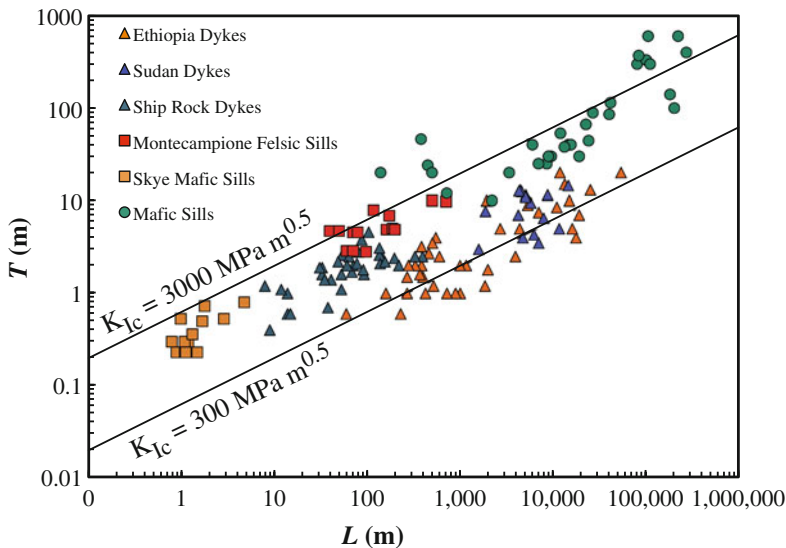


**Fig. 5** Dimensional data for large mafic sills (multiple sources), felsic-intermediate sills (Montecampione—Corazzato and Groppelli 2004; Skye—Walker 1993) and mafic dykes (Ship Rock—Delaney and Pollard 1981; Ethiopia—Schultz et al. 2008b). *Black curves* are fit lines for LEFM conditions dominated by fracture toughness (Eq. 3) and for fracture toughness values $K_{Ic}$— 3000 and 300 MPam$^{0.5}$. See text for further discussion

length (Fig. 5). Therefore, LEFM accounts satisfactorily for the scaling of these intrusion types if large effective $K_{Ic}$ values can be accounted for by scale effects (e.g., Olson 2003), fracture network branching (e.g., Gudmundsson 2011a) or cooling/solidification at fracture tips (viz., tip screen out; Smith et al. 1987). Furthermore, this model is favoured relative to the LEFM model under conditions of uniform magma pressure, which is at odds with the data because it predicts $a \sim 1$ (Olson 2003). A toughness-dominated model is also favoured relative to models that consider viscous flow to be predominant because the magma viscosity range required to bracket the data is implausibly high (Cruden et al. 2009).

For completeness, large mafic sills have been included in Fig. 5 and contribute to a well-defined RMA slope for the sheets and sills data array with $a = 0.57 \pm 0.02$ (Table 1). However, RMA analysis of mafic sills with $L > 1000$ m alone gives a slope $a = 0.85 \pm 0.1$, which is influenced by the presence of thick sills with $L > 100$ km that lie above the bounding curve plotted in Fig. 1a. As discussed above, mafic sills with L ≫ 1 km likely interact with the surface and their emplacement is discussed together with laccoliths below.

## 4.2 Intrusions that Do Interact with Earth's Surface

The growth of intrusions with $L \gg H$ involves vertical displacement of overlying strata and ultimately the creation of positive surface topography (Hamilton 1965; Corry 1988; Cruden 1998; Galland and Scheibert 2013). Because their growth does not normally require deflection of rock units below the level of emplacement, intrusions with $L \gg H$ are characterised by asymmetric geometries in cross section (i.e., flat floors, curved roofs), which contrasts with the symmetric deflection of strata above and below intrusions with L ≪ H (Fig. 6; Koch et al. 1981). In addition to uplift of overlying strata, a further manifestation of interaction with the surface is the tendency for some sill tips to curve upwards during sill growth, resulting in the formation of
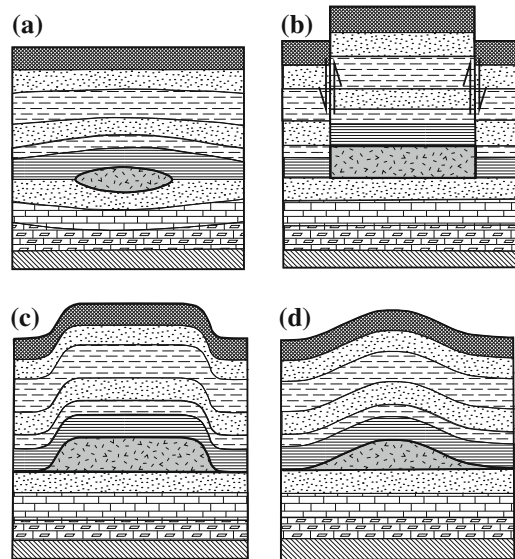


**Fig. 6** Conceptual models for host rock deformation associated with emplacement of sills and laccoliths (after Koch et al. 1981). **a** Emplacement of an initial sill with H ≫ L and no interaction with Earth's surface. **b** Vertical growth of a laccolith by plastic failure on ring faults and roof uplift (a.k.a. punched laccolith). **c** Vertical and horizontal growth of a laccolith by the rolling hinge mechanisms, which requires intra layer slip in the roof rocks. **d** Classical model of laccolith growth by elastic displacement of roof rocks under a thin, clamped, circular elastic plate mechanical regime. See text for further discussion

saucer-shaped intrusions in shallow sedimentary basins (Malthe-Sørenssen et al. 2004; Thomson and Hutton 2004; Polteau et al. 2008; Magee et al. 2016; Planke et al. this volume).

Several end-member mechanisms for the growth of laccoliths have been proposed (e.g., Hunt et al. 1953; Sneddon and Lowengrub 1969; Pollard and Johnson 1973; Koch et al. 1981; Corry 1988; Price and Cosgrove 1990; Zenzri and Kerr 2001; Horsman et al. 2010). Most analytical models start with the emplacement of an initial sill (Fig. 6a), followed by vertical inflation (Fig. 6b–d). Such models can also be employed to estimate the critical conditions (L, H, driving pressure, etc.) required to initiate the so-called sill-to-laccolith transition. Gilbert's (1877) original concept for laccolith emplacement envisaged that uplift of overlying rigid strata was facilitated by a ring fracture (Fig. 6b) and that the final

thickness of the flat-topped intrusion was a consequence of the balance between magma overpressure, the weight of the overlying rocks and friction on the fault. Corry (1988) has termed these intrusions punched laccoliths. Also based on fieldwork in the Henry Mountains, Hunt et al. (1953) introduced the rolling monoclinal flexure (hinge) model for laccolith emplacement, subsequently modelled by Koch et al. (1981) to incorporate interlayer sliding, which again predicts a flat topped geometry and also the upwarping of strata adjacent to the intrusion margin (Fig. 6c). Building on elastic plate theory (e.g., Sneddon and Lowengrub 1969), the third end-member model type for laccolith growth (Fig. 6d) is based on vertical deflection of a circular, thin elastic plate (e.g., Perkins and Kern 1961; Pollard and Johnson 1973; Zenzri and Kerr 2001). For example, Pollard and Johnson (1973) adopted a solution for a thin, clamped, circular elastic plate to model laccolith growth and the sill-to-laccolith transition. This model, which has been used extensively to estimate driving pressures and intrusion thicknesses (e.g., Price and Cosgrove 1990; McCaffrey and Petford 1997), predicts the bell-jar shape that has come to be synonymous with laccoliths in textbooks (Fig. 6d).

Common to these analytical solutions for laccolith growth is that $L$ must be assumed prior to calculation of the final intrusion thickness. Hence, in these models the sill-to-laccolith transition does not emerge spontaneously from the dynamics because the solution lacks a moving propagation condition at the sill (then laccolith) tip. Furthermore, although the punched laccolith and rolling hinge models predict laccoliths with flat tops, the elastic plate model predicts bell jar-shaped cross sections, which are generally not supported by field observations.

Analogue and numerical studies of sill and laccolith emplacement and growth overcome some of the limitations of analytical solutions (e.g., Dixon and Simpson 1987; Roman-Berdiel et al. 1995; Mathieu et al. 2008; Polteau et al. 2008; Galland et al. 2006; Kavanagh et al. 2006, 2015; Menand 2008; Galland and Scheibert 2013). While such experimental studies provide considerable insight into the dynamics and structural evolution of sills and laccoliths (see Galland et al. this volume, for a comprehensive review), like the analytical models, they are still not able to predict the observed $L$-$T$ (and $V$) scaling of intrusions.

## 5 Modelling the Growth of Sills and Laccoliths

In order to further explore the mechanical significance of the $L$-$T$ scaling of sills and laccoliths, as well as their leading-order geometrical attributes, Bunger and Cruden (2011a) developed an elastic, thin plate model that also takes into account a moving fracture propagation condition at the sill/laccolith tip, fluid flow within the intrusion and the influence of the magma weight on intrusion growth and shape. Key features of the model are summarised in Fig. 7a. A circular crack at depth, $H$ is fed by a central conduit at a volumetric flow rate, $Q_o$, which depends implicitly on magma overpressure. The problem is then to determine the fluid pressure, crack opening $w$, and radius $R$ as a function of time. The resulting mathematical model comprises a continuity equation for fluid flow, and equations for fluid flow rate, an elastic plate and crack tip propagation, and suitable initial and boundary conditions. The combined solutions to these coupled equations, including details of the required numerical routine are detailed in Bunger and Cruden (2011a, b).

The model results are presented using scaling factors that relate the dimensional intrusion opening, $w$, radius, $R$, net pressure, $p$, and radial fluid flux, $q$, to equivalent dimensionless values $\Omega$, $\gamma$, $\pi$, and $\Psi$, respectively. The equations are simplified by using the alternative host rock and magma parameters:

$$E' = \frac{E}{1 - v^2}, \quad \mu' = 12\mu, \quad K' = 4\left(\frac{2}{\pi}\right)^{\frac{1}{2}} K_{Ic}, \tag{4}$$

where $\mu$ is magma dynamic viscosity. Two dimensionless groups, or evolution parameters,
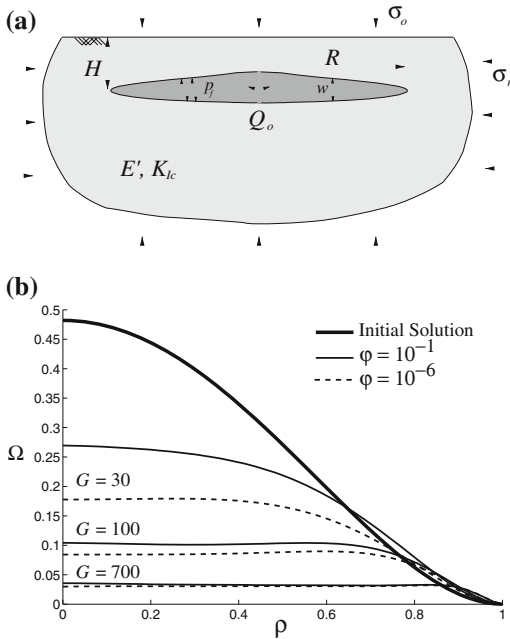
**Fig. 7** **a** Sketch of the sill and laccolith growth model introduced by Bunger and Cruden (2011a). See text for explanation of symbols. **b** Profiles of the dimensionless opening, $\Omega$, across a dimensionless half width of the intrusion as a function of dimensionless time, expressed by the evolution parameter, $G$. The *upper dark curve* is the initial solution, which corresponds to the elastic plate solution illustrated in Fig. 6d. With increasing time and $G$ the outwardly growing intrusion develops a flat top and uniform thickness

and two characteristic times describe the behaviour of the model:

$$G_m = \frac{E'^2 H^3 \mu'}{K'^2 t}, \quad G = \frac{\rho_m g Q_0 t}{H^{3/2} K}, \quad (5)$$

$$t_m = \frac{E'^2 H^{3/2} \mu'}{K'^3}, \quad t_p = \frac{H^{3/2} K'}{\rho_m g Q_0}, \quad (6)$$

where $G_m$ describes the behaviour when magma viscosity dominates the dynamics and $G$ describes the dynamics when magma weight, $\rho_m g$ dominates, and $t_m$ and $t_p$ are the corresponding characteristic times.

When $t_m$ is large in comparison to time, $t$, $G_m$ is also expected to be large, indicating that fluid pressure gradients will be large and the system will be "viscosity dominated." When $t \gg t_m$, $G_m$

becomes vanishingly small and the system is referred to as "toughness dominated" (e.g., Savitsky and Detournay 2002; Detournay 2004). The system therefore evolves from viscosity to toughness dominated as time increases relative to $t_m$. Simultaneously $t$ will increase relative to $t_p$, which is the characteristic time for the transition from an early regime when the influence of magma weight is negligible to a later time when its influence is significant, as implied by the evolution parameter $G$. A "trajectory" parameter $\varphi = t_m/t_p$ can be defined, which plays the role of a dimensionless viscosity. $\varphi$ indicates the time required for viscous effects to vanish and for magma weight to become dominant, which is predicted to occur very early on in the evolution of real intrusions (Bunger and Cruden 2011a).

The effects of $G$ (and time) and $\varphi$ on the dimensionless opening profile of the model intrusion are illustrated in Fig. 7b, where $\rho = r/R$ is the dimensionless horizontal distance from the centre. Model intrusion growth can be characterised by a transition from a bell jar shaped, uniformly pressurised solution when $G \ll 1$, to a solution for $G \gg 1$ in which the thickness is uniform over most of the extent of the intrusion. The bell jar shape when $G \ll 1$ essentially corresponds to the well-known solution of Pollard and Johnson (1973). When $G \gg 1$ the intrusion becomes increasingly flat topped over time as $G$ increases, becoming a thin disk by $G = 1000$. The role of $\varphi$ is to slow down the transition from the bell jar shaped plate solution to the flat-topped solution. Corrected numerical solutions for $\Omega$ and $G$ are tabulated in Bunger and Cruden (2011b) for values of $\varphi = 10^{-1}$ and $\varphi = 10^{-6}$.

The tabulated values for $\Omega$ and $G$, together with emplacement depth and host rock and magma parameters (Eq. 4) can be used to determine the dimensional intrusion radius and opening from:

$$w = \left(\frac{GK'^2}{E'g\rho_m}\right)^{\frac{1}{2}} \Omega, \quad R = \left(\frac{GE'H^3}{g\rho_m}\right)^{\frac{1}{4}} \gamma. \quad (7)$$

By equating $T = w$ and $L = 2R$, results from Eq. 7 can be used to model the growth of laccoliths and sills over time (expressed as

increasing $G$) in log $T$ versus log $L$ space and to explore the roles of emplacement depth and host rock fracture toughness and rigidity on intrusion shape and aspect ratio. Because the equation for $G$ contains the expression $Q_o t = V$, intrusion growth times can be estimated for different volumetric flow rates and host rock properties and emplacement depths; conversely, if $t$ is known independently (e.g., from geochronology) then volumetric flow rate can be estimated for different conditions. Usually both $Q_o$ and $t$ are unknown, in which case the outcome of increasing $V$ can be explored while varying host rock properties and emplacement depths.

Growth curves for laccoliths and sills predicted by the model follow paths with a common shape in log $T$ versus log $L$ space (Fig. 8).
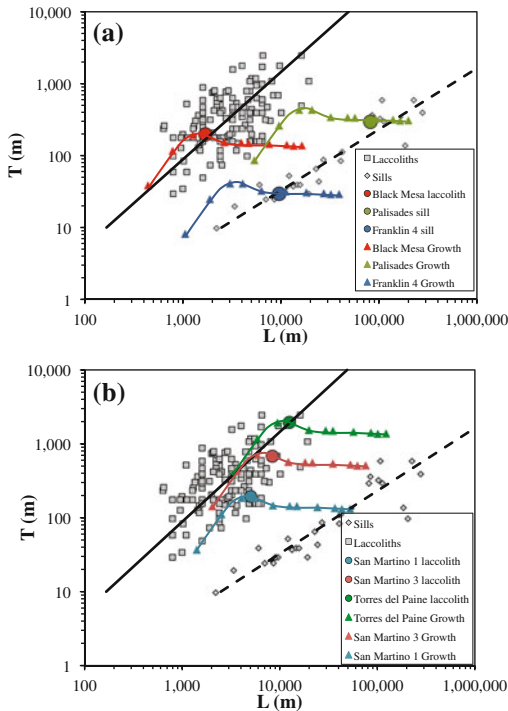


**Fig. 8** Geometric growth curves of some natural laccoliths modelled using the model of Bunger and Cruden (2011a) and plotted in log $T$ versus log $L$ space. Dimensional data for laccoliths and sills, and scaling lines from Fig. 1 are included for reference. **a** Growth scenarios for the Black Mesa laccolith, Palisades sill and Franklin 4 sill. **b** Growth scenarios for the San Martino 1 and 2 laccoliths and Torres del Paine pluton. See Table 2 and text for model parameters and further discussion

Starting at $G = 0.1$, initial growth follows a trajectory with a similar slope to the power law scaling curve for laccoliths, meaning that during this phase it thickens faster than it lengthens. The intrusion reaches a maximum thickness between $G = 5$ and 10, at which point it has the typical flat-topped and steep sided morphology of laccoliths. After this stage, as the intrusion continues to lengthen, $T$ decreases as $G$ approaches 30. For $G = 70$–1500 the thickness remains essentially constant as it approaches an asymptotic value. For $G > 100$ the intrusion has the high aspect ratio, uniform thickness and tapered margin characteristic of sills.

Here we explore the effects of varying $H$, $K_{Ic}$, and $E'$ on the evolution of $T$, $L$ and $V$ over time. We also attempt to constrain the growth histories and conditions for selected laccoliths and sills in nature.

## 5.1 Influence of Emplacement Depth and Bulk Country Rock Mechanical Properties

When $H$, $K_{Ic}$, or $E'$ are varied, the intrusion growth trajectory will be shifted up down or sideways on a log $T$ versus log $L$ plot but its shape remains unchanged. This is illustrated in Fig. 8 for different case studies of natural intrusions, detailed below.

The effect of increasing the emplacement depth is to move the growth trajectory curves from left to right in the log $L$ direction, as expected from the dimensional radius, $R$, predicted by Eq. 7. Hence, keeping $G$ and the country rock properties equal, deeper sills and laccoliths will have greater widths and larger aspect ratios, which is consistent with the findings of analogue experiments on sills and laccoliths (Dixon and Simpson 1987; Roman-Berdiel et al. 1995) and some geophysical and numerical modelling constraints (Polteau et al. 2008). Not accounted for in the Bunger and Cruden (2011a) model is the concept of the effective overburden thickness, $T_e$. Pollard and Johnson (1973) introduced $T_e$ in order to account for the mechanical behaviour of multilayered rocks overlying a growing sill or laccolith. If each layer boundary is able to slide freely they found that $T_e \sim 1/7H$ to

2/3$H$ for examples studied in the Henry Mountains, Utah. Evidence for layer parallel sliding and detachments has since been documented in the roof rocks of laccoliths in the Henry Mountains (Wilson et al. 2016). Hence sills and laccoliths emplaced into thick sequences of mechanically layered host rocks can exhibit growth histories and aspect ratios characteristic of shallower depths.

When $K_{Ic}$ is increased, growth trajectory curves are shifted vertically towards higher $T$ values, consistent with the prediction for the dimensional opening, $w$, in Eq. 7. Hence when all else is equal, high fracture toughness country rocks will favour thicker, lower aspect ratio intrusions.

The country rock stiffness parameter has a counteracting effect on both $H$ and $K_{Ic}$, such that an increase in $E'$ will move the growth trajectory curve from top left to bottom right, owing to the fact that $E'$ appears in the denominator and numerator of the equations for $w$ and $R$, respectively (Eq. 7). Hence when all else is equal, high stiffness country rocks will favour thinner, wider, higher aspect ratio intrusions. The magma density, $\rho_m$, is also a factor in Eq. 7 and higher values will shift growth curves downwards. However, the effect of $\rho_m$ is minor compared to that of $K_{Ic}$ and $E'$.

## 5.2 Selected Case Studies of Sills and Laccoliths

Using the growth trajectories described above it is possible to match growth curves for specific examples in nature. However, any solution for a given sill or laccolith will not be unique because three parameters (four including density) can be varied to achieve the desired outcome. The approach we have taken here is to vary $E'$ and $K_{Ic}$ such that the known $T$ and $L$ dimensions are achieved for the appropriate $H$ (if known) and $G$-value. We have taken $G \sim 10$ to be representative of laccoliths and $G \sim 100$–300 to be likely end points for sills. The most favoured growth curve will be one that satisfies these constraints while keeping $K_{Ic}$ and E' as close as possible to accepted values (Fig. 8, Table 2). For reference, the typical range of laboratory-derived values of

$K_{Ic}$ and $E'$ are 0.5–2 MPam$^{0.5}$ and $1.04 \times 10^3$–$8.3 \times 10^4$ MPa, respectively (Olson 2003). Delaney and Pollard (1981) and Olson (2003) report values estimated from the Ship Rock dyke, Colorado Plateau, of $K_{Ic} = 40$–4000 MPam$^{0.5}$ and $E' = 2.5 \times 10^3$–$2.5 \times 10^4$ MPa, which highlight the current uncertainty in field-scale versus laboratory-scale rock property characterisation.

### 5.2.1 Black Mesa Laccolith, Henry Mountains, Utah

We start with modelling possible growth histories for the Tertiary age Black Mesa laccolith (Johnson and Pollard 1973; de Saint Blanquat et al. 2006). The first three scenarios presented in Table 2 result in identical growth trajectories, arriving at the same $L$-$T$ dimensions when $G = 10$ (Fig. 8a). The first scenario starts with an emplacement depth $H = 2500$ m derived from stratigraphic constraints (Johnson and Pollard 1973) and is optimised to keep $K_{Ic}$ within the range of laboratory values. In this case the desired dimensions are reached when $K_{Ic} = 1.2$ MPam$^{0.5}$ and $E' = 0.01$ MPa, so the country rocks must have anomalously low elastic stiffness to achieve sufficient vertical growth at the known emplacement depth. In the second scenario, following Johnson and Pollard (1973), we adopt an effective elastic thickness $T_e = 0.15$ $H = 375$ m and find that the correct dimensions can be achieved when $K_{Ic} = 20$ MPam$^{0.5}$ and $E' = 2.5$ MPa, which again requires a very low country rock elastic stiffness. Finally, we explore a scenario that is optimised for $E'$ and find that Black Mesa growth could have occurred for acceptable field-scale values $K_{Ic} = 400$ MPam$^{0.5}$ and $E' = 1000$ MPa but the required emplacement depth, $H = 50$ m is 2450 m short of the known value. Modelling the final dimensions of the Black Mesa laccolith therefore requires emplacement into country rocks that are extremely compliant ($E' \sim 1000$ times lower than normal values) or with a very low effective overburden thickness, in this case $T_e \sim 0.02H$.

One limitation of the present modelling approach is that it does not consider plastic yielding of the country rocks. The Black Mesa

**Table 2** Sill and laccolith growth scenarios

| Intrusion (scenario) | Type | $L$ (m) | $T$ (m) | $G$ | $H$ (m) | $K_{Ic}$ MPam$^{0.5}$ | $E'$ MPa | $V$ (m$^3$) | $Q_e$ m$^3$/s | $t$ (year) | References | Comments |
|---|---|---|---|---|---|---|---|---|---|---|---|---|
| Black Mesa (1) | Laccolith | 1700 | 200 | 10 | 2500 | 1.2 | 0.01 | $2.0 \times 10^8$ | 0.1 | 66 | Johnson and Pollard (1973), Blanquat et al. (2006) | Estimated emplacement depth |
| Black Mesa (2) | Laccolith | 1700 | 200 | 10 | 375 | 20 | 2.5 | $2.0 \times 10^8$ | 0.1 | 66 | Johnson and Pollard (1973), de Saint Blanquat et al. (2006) | Effective thickness $T_e = 0.15H$ |
| Black Mesa (3) | Laccolith | 1700 | 200 | 10 | 50 | 400 | 1000 | $2.0 \times 10^8$ | 0.1 | 66 | Johnson and Pollard (1973), de Saint Blanquat et al. (2006) | Optimised for $E'$, $T_e = 0.02H$ |
| Black Mesa (4) | Laccolith | 1700 | 10 | 10 | 55 | 20 | 1000 | $2.3 \times 10^7$ | 0.1 | 3.3 | Johnson and Pollard (1973), de Saint Blanquat et al. (2006) | Single pulse, $T_e = 0.022H$ |
| San Martino 1 (1) | Laccolith | 5000 | 200 | 10 | 2200 | 15 | 1.5 | $2.0 \times 10^9$ | 0.1 | 648 | Rocchi et al. (2002) | Estimated emplacement depth |
| San Martino 1 (2) | Laccolith | 5000 | 200 | 10 | 250 | 400 | 1000 | $2.0 \times 10^9$ | 0.1 | 648 | Rocchi et al. (2002) | Optimised for $E'$, $T_e = 0.11H$ |
| San Martino 3 | Laccolith | 8300 | 700 | 10 | 1900 | 150 | 10 | $1.6 \times 10^{10}$ | 0.1 | 5200 | Rocchi et al. (2002) | Estimated emplacement depth |
| Torres del Paine (1) | Laccolith | 12400 | 2000 | 10 | 2500 | 700 | 30 | $2.5 \times 10^{11}$ | 0.04 | 91500 | Michel et al. (2008), Leuthold et al. (2012) | Estimated emplacement depth |
| Torres del Paine (2) | Laccolith | 12400 | 100 | 10 | 600 | 300 | 2000 | $5.7 \times 10^9$ | 0.04 | 4600 | Michel et al. (2008), Leuthold et al. (2012) | Single pulse, $T_e = 0.24H$ |
| Palisades | Sill | 80000 | 300 | 300 | 4000 | 200 | 50 | $2.0 \times 10^{12}$ | 10 | 6350 | Walker (1969) | Estimated emplacement depth |
| Franklin 4 | Sill | 9500 | 30 | 100 | 1000 | 6 | 5 | $2.5 \times 10^9$ | 10 | 7.9 | Robertson and Baragar (1972), Bédard et al. (2012) | Minimum emplacement depth |

laccolith is partially bounded by a steep fault on its southeast side (Fig. 4b), indicating failure of overburden rocks during vertical inflation (de Saint Blanquat et al. 2006). We suggest that plastic failure of overburden rocks during laccolith emplacement could result in significant reduction in $T_e$ or $E'$ as a consequence of reducing the amount of elastic bending required to accommodate vertical inflation. Punched laccoliths (Fig. 6b; Gilbert 1877) and bysmaliths (Daly 1905) are examples of intrusion types that form by this process.

Another limitation of our modelling approach is that it does not allow for the emplacement of pulses and stacking of sheets, which are thought to have played a role in the growth of the Black Mesa laccolith (de Saint Blanquat et al. 2006) and many other intrusions. In order to attempt to take this into account for the Black Mesa laccolith, we have explored a fourth scenario for the conditions required for the emplacement of a 10 m thick sheet with a width, $L \sim 1700$ m equal to the final intrusion (Table 2). This corresponds to modelling one of 20 arbitrary pulses of equal thickness that will eventually be stacked to form the final laccolith. The result presented here has been optimised for a large $E' = 1000$ MPa and relatively small $K_{Ic} = 20$ MPam$^{0.5}$. For these parameters we find that that the effective depth must be 55 m or $T_e = 0.022H$. A general conclusion we can draw for the Black Mesa laccolith is that either the effective overburden thickness or the elastic stiffness of the overburden must have been very low, even if it grew by injection of multiple thin pulses. This points to host rock plasticity as an important factor for its emplacement and growth.

## 5.2.2 San Martino Laccoliths, Elba Island

The San Martino 1 and 3 intrusions are part of a stack of Miocene age (Tortonian-Messinian) laccoliths that are well exposed on central Elba Island, Italy (Rocchi et al. 2002, 2010). They are emplaced into a layered and thrust stacked sequence of Cretaceous to Eocene flysch. The vertical and horizontal dimensions of the laccoliths are well constrained by field mapping and

their depths of emplacement have been estimated from their stratigraphic position (Table 2). Growth trajectories for both laccoliths (Fig. 8b) can be matched to their dimensions without making adjustments for depth and for reasonable field-scale values of $K_{Ic} = 15–150$ MPam$^{0.5}$ but require low values of $E' = 1.5–10$ MPa. Higher values of $E'$ could be offset by $T_e < H$ and larger $K_{Ic}$ as in scenario 2 for San Martino 1 (Table 2). In this case $T_e = 0.11H$, which approaches the range of effective thicknesses proposed by Pollard and Johnson (1973). Hence the model accounts for the scaling for the Elba laccoliths reasonably well given the known mechanical layering of the overburden rocks. However, the role of plastic yielding cannot be ruled out and is supported by local evidence for intrusion-related faulting in the country rocks (Westerman et al. this volume).

## 5.2.3 Torres Del Paine Pluton, Patagonia

In order to assess the emplacement of a very large laccolith, we have modelled the growth of the Miocene age (Tortonian) Torres del Paine granite, Patagonia, Chile (Skarmeta and Castelli, 1997). The tabular Torres del Paine pluton comprises three compositionally distinct, 400–800 m thick sheets of the Paine granite, which are underlain by the >500 m thick Paine Mafic Complex (Michel et al. 2008). Both the granite units and the mafic complex are themselves made up of multiple pulses of variable thickness. Emplacement occurred into layered and folded Cretaceous flysch at a depth estimated from geobaromentry of 2–3 km (Michel et al. 2008). The estimated 88 km$^3$ of the entire plutonic complex is thought to have grown from the top down (underplating) over a period of $162 \pm 11$ ka (Leuthold et al. 2012) and the granitic units were emplaced over $90 \pm 40$ ka (Michel et al. 2008).

Assuming continuous emplacement, we first model the growth trajectory for the granitic part of the Torres del Paine pluton without making any adjustment for depth and for a reasonable field-scale value of $K_{Ic} = 700$ MPam$^{0.5}$ (Fig. 8b; Table 2). As in the other laccolith examples

above, growth to the correct dimensions at the known emplacement depth cannot be achieved without adopting a relatively low host rock stiffness, here $E' = 30$ MPa. In the case of Torres del Paine, this could partly be explained by thermal softening of the host rocks, which is supported by the presence of a well-developed contact metamorphic aureole (Putlitz et al. 2001). In a second scenario we consider injection of a 100 m thick pulse with $L$ spanning the entire width of the pluton (Table 2). In this case we find that emplacement and growth can occur for geologically reasonable values of both $K_{Ic}$ and $E'$ if $H = 600$ m. The latter corresponds to $T_e = 0.24H$, which is well within the range estimated by Pollard and Johnson (1973). These findings strongly support the field-based interpretation that the Torres del Paine pluton grew by vertical stacking of multiple sheet-like pulses (Michel et al. 2008; Leuthold et al. 2012).

### 5.2.4 Palisades Sill, Eastern USA and Franklin Sills, Nunavut, Canada

Finally, we consider two mafic sills in order to assess growth up to larger values of $G$ and $L$ (Fig. 8a; Table 2). The Jurassic age Palisades sill intruded layered sedimentary and volcanic rocks of the Mesozoic Newark Basin, eastern USA (Walker 1969; Puffer et al. 2009). Stratigraphic arguments and thermal modelling suggest an estimated emplacement depth of 3–4 km (Walker 1969; Shirley 1987). We also examine one of the mafic sills that make up part of the Neoproterozoic Franklin large igneous province, Victoria Island, Canada (Robertson and Baragar 1972; Bédard et al. 2012). The sills intruded gently folded layered sedimentary rocks and basalt flows of the Neoproterozoic Shaler supergroup at emplacement depths ranging between $\sim 1$ and 4 km (Bédard et al. 2012). We focus on Franklin Sill 4 (see Fig. 2 in Robertson and Baragar 1972 for location), which we assume to have been emplaced at a minimum depth of 1000 m.

Growth trajectories for both sills show that their final dimensions can be modelled for $G = 300$ (Palisades) and 100 (Franklin 4) using their

estimated or minimum emplacement depths and for reasonable field-scale values of $K_{Ic}$ (Fig. 8a; Table 2). In both cases we find that the country rocks must have low values of elastic stiffness. For the Palisades sill, this could be offset by replacing $H$ with a lower $T_e$, given the strongly layered nature of the host rocks, and by considering emplacement by several pulses, for which there is debated field and petrological evidence (Walker 1969). In the case of Franklin 4, low values of $E'$ would be compatible with host-rock plasticity and failure, which is consistent with detailed mapping by Bédard et al. (2012) who documented significant interaction between pre-existing faults and sills during their emplacement and propagation through the crustal section.

### 5.3 Timescales of Laccolith and Sill Growth

Given that the final intrusion volume can be estimated from $T$ and $L$ we also can assess likely emplacement times by assuming typical magma volumetric flow rate values ($Q_o$). These times can be compared to independent estimates of emplacement duration from geochronology or thermochronology and cooling calculations. The value of $Q_o = 0.1$ m$^3$/s ($\sim 0.003$ km$^3$/yr) adopted for the Black Mesa and San Martino laccoliths is based on representative and conservative magma volumetric flow rate values estimated for felsic-intermediate intrusions and eruptions (Petford et al. 2000; White et al. 2006; de Saint Blanquat et al. 2011; Menand et al. 2015). This gives an emplacement time of 66 years for the Black Mesa laccolith, which is close to the maximum value of 100 years estimated by de Saint Blanquat et al. (2006) based on thermal modelling. Using the volumetric flow rate value above San Martino 1 and 3 laccoliths could have been emplaced over $\sim 600$ to $\sim 5000$ years, respectively. However, Rocchi et al. (2002) estimated a filling time for the combined San Martino laccoliths of $\sim 100$ years based on an estimated dyke-fed magma ascent rate of $3 \times 10^{-3}$ m/s. Increasing $Q_o$ to 5 m$^3$/s would result in a combined emplacement time for both

laccoliths of $\sim$100 years, consistent with this previous estimate, although the required volumetric flow rate ($\sim$0.1 km$^3$/year) is very high compared to known eruption and emplacement rates of felsic magmas (White et al. 2006; de Saint Blanquat et al. 2011).

Precise geochronology indicates that the granitic part of the Torres del Paine pluton was emplaced over 90 ± 40 Ka (Michel et al. 2008). Using this as a constraint, continuous growth of the pluton requires a magma flux $Q_o \sim$ 0.04 m$^3$/s ($\sim$0.001 km$^3$/year), which is also consistent with previous estimates from other intrusions and eruptions (White et al. 2006; de Saint Blanquat et al. 2011). Note that this does not take into consideration the possibility of a time lag or repose period between magma pulses (e.g., Cruden 2006; White et al. 2006). In such cases and when the time lag is relatively long compared to the pulse emplacement time, $Q_o$ could be much larger.

There are no geochronological constraints for the emplacement duration of the Palisade and Franklin 4 sills. Thermal modelling of the Palisades sills indicates magma solidification over $\sim$1000 years (Shirley 1976), which provides a minimum estimate of the emplacement time. Since both mafic sills were emplaced during high magma flux mantle melting events, we assume a conservative value of $Q_o \sim$ 10 m$^3$/s ($\sim$0.3 km$^3$/year), corresponding to the upper end of mafic magma eruption rates (White et al. 2006; de Saint Blanquat et al. 2011). This gives continuous emplacement times for the Palisades and Franklin 4 sills of $\sim$6000 and $\sim$8 years, respectively.

## 6 Discussion

### 6.1 Bifurcation Between Laccolith and Sill Growth Histories

Current models do not predict the observed bifurcation between mafic sills and laccoliths at $L \sim$ 500 m. Neither emplacement depth nor composition provides an explanation because laccoliths and large mafic sills are similar in this

regard. However, it is clear that both intrusion types follow different evolutionary pathways with laccoliths forming in a thickening (roof lifting, $a > 1$) dominated regime and large mafic sills forming in a lengthening (horizontal propagation, $a < 1$) dominated regime. Below $L \sim$ 500 m and $T \sim$ 10 m tabular intrusion types are indistinguishable.

The modelling discussed in the previous sections shows that laccoliths and large mafic sills share a common evolutionary path at early growth stages, initially thickening faster than they lengthen (Bunger and Cruden 2011a). However, laccoliths appear to stop growing at low $G$, which may occur due to cessation in magma supply and/or freezing, resulting in a low aspect ratio intrusion ($L/T < 10$). If more magma is available, the additional magma weight is capable of driving the intrusion outwards with constant thickness to large aspect ratios, stopping at large $G$ when magma supply ends or solidification occurs. Hence, large mafic sill formation is favoured in tectonic settings that generate large volumes of hot melt, such as during continental breakup and Large Igneous Province development (e.g., Ernst et al. 2005). Conversely, laccoliths tend to form in settings where magma supply is restricted, such as intraplate settings. We therefore suggest that the main control on the observed bifurcation in scaling behaviour is related to tectonic setting and available magma supply, rather than depth, composition or viscosity.

An alternative or complementary cause of the data bifurcation is that laccoliths and plutons tend to grow incrementally by stacking of sheets (e.g., Cruden and McCaffrey 2001; Coleman et al. 2004; Horsman et al. 2010; Rocchi et al. 2010; Annen 2011; Menand 2011), consistent with growth dominated by vertical inflation. By contrast, most sills are thought to represent one or a small number of intrusion events (e.g., Hergt and Brauns 2001; Marsh 2004), consistent with growth dominated by horizontal elongation. Formation of a laccolith or pluton by sheet stacking would result in a vertical growth trajectory on a log $T$ versus log $L$ plot with $a \gg 1$ (see Fig. 7 in Cruden and McCaffrey 2001 and Fig. 8 in Rocchi et al. 2010). However, it is

currently unclear why such a two-stage growth history would result in the observed power-law scaling of laccoliths and plutons, or the bifurcation in the scaling data at $L \sim 500$ m.

## 6.2    Intrusions Too Deep to Interact with Earth's Surface

Polyphase granitic to dioritic plutons and layered mafic intrusions are typically emplaced at upper to mid-crustal depths (2–15 km) into both layered and crystalline host rocks. Multiple processes likely operate during their emplacement, including brittle and ductile wall-rock deformation, stoping and assimilation (Paterson et al. 1996; Cruden 2006). However, space for most plutons and layered mafic intrusions is thought be created by vertical displacement of wall rocks, which at the shallowest depths can occur by roof lifting but below $\sim 3$ km is likely dominated by floor depression (e.g., Myers 1975; Cruden 1998; Wiebe and Collins 1998; Brown and McClelland 2000). The process of floor depression is driven by a periodic exchange of material (melt) from a partially molten source region in the lower crust

to the growing pluton in the mid- to upper crust (Cruden and McCaffrey 2001; Cruden 2006) or between an upper and a lower chamber (Clough et al. 1909; Myers 1975). The cumulative downward displacement of the intervening crustal column requires large-scale brittle or ductile deformation depending on emplacement depth. Although many plutons and layered mafic intrusions are constructed by multiple pulses (Glazner et al. 2004; de Saint Blanquat et al. 2011; Annen 2011), which could be treated as individual sill emplacement events (Menand 2011), the requirement of large-scale plasticity to make space indicates that a single LEFM-based model cannot be used to predict their observed $a < 1$ power-law scaling. Acknowledging the roles of local and far-field deformation, the underlying control on the dimensions and scaling of plutons and layered mafic intrusions likely originates in the lateral extent and melt productivity of underlying magma source region, which will determine both the length and thickness of the resulting intrusion, respectively (Cruden 2006; Scaillet and Searle 2006). The transition from laccoliths with $a > 1$ to plutons and layered mafic intrusions with $a < 1$ therefore reflects an
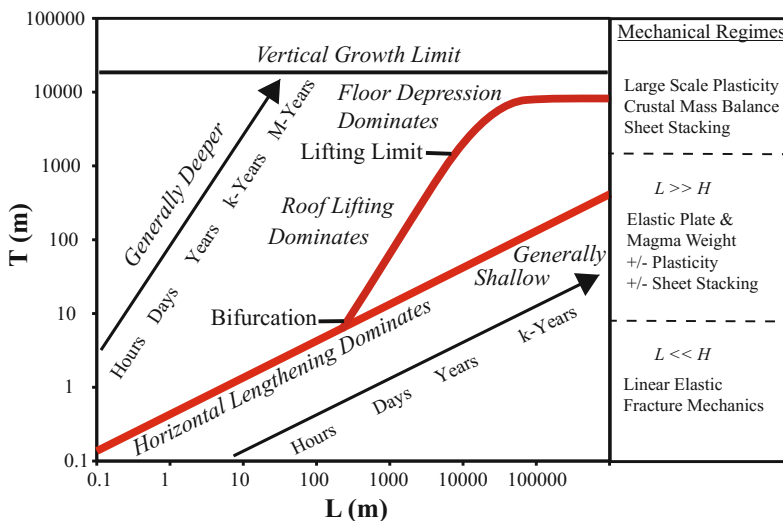


**Fig. 9** Regime diagram for tabular intrusion scaling and growth mechanisms in log $T$ versus log $L$ space. *Red curves* summarize the dimensional scaling relationships (Fig. 1) for different classes of intrusion. *Arrows* indicate

tendencies for increasing emplacement depth and time. Dominant mechanical regimes for emplacement are indicated at *right* with approximate boundaries or thresholds based on intrusion thickness and depth

increase in the depth of emplacement and a transition from an intrusion regime where interaction with the surface is important to one where interaction with the underlying source region controls the leading order behaviour (Fig. 9).

Batholiths and large layered mafic intrusions are composite bodies built over long time periods. The building blocks of batholiths are plutons whereas large layered mafic intrusions comprise multiple sheet-like bodies enclosed within a single envelope (Cawthorn 1996; Saumur and Cruden 2016). Batholiths and large layered mafic intrusion are therefore emplaced by multiple processes and grow by a combination of vertical stacking and lateral accretion. The final size and shape of these structures is likely controlled by the underlying tectonic regime. The upper bound on $T \sim 10$ km corresponds to 1/3–1/4 of the thickness of normal or over-thickened continental crust and likely reflects a growth limit related to long-term magma supply in arc, extensional and plume settings.

# 7 Towards a General Framework for Tabular Intrusion Emplacement and Growth

The geometric scaling of tabular intrusions provides a useful framework for defining and understanding three first-order magma emplacement regimes in the crust (Fig. 9). Small, horizontal tabular intrusions with $L \sim 5$–1000 m are characterised by a power law scaling with $a \sim 0.5$. These intrusions satisfy the condition $L < H$ and their emplacement can be explained by LEFM if field-scale fracture toughness values are allowed to exceed laboratory values.

When $L \sim 500$–1000 m there is a pronounced bifurcation in the scaling data with shallow, large mafic sills defining one branch with $a < 1$, and laccoliths defining second branch with $a > 1$ (Fig. 9). The emplacement of both laccoliths and large mafic sills occurs in a regime where $L > H$, whereby space is made predominantly by roof lifting. The geometry and scaling of laccoliths and large mafic sills can be adequately explained by elastic plate models that take into account a propagation condition at the crack tip and the role of magma weight (Bunger and Cruden 2011a). As with small sheets with L < H modelled by LEFM, these models require country rocks to have large field-scale fracture toughness values compared to laboratory values. More importantly, when attempting to match the dimensions of specific examples in nature we also find that the host rocks must have anomalously low elastic stiffness and/or the effective emplacement depth must be much lower than the known depth. The latter can be partly explained by the mechanical behaviour of well-layered overburden rocks (Pollard and Johnson 1973). In some cases (e.g., Torres del Paine pluton) the low stiffness of the country rocks might also be accounted for by thermal softening. However, in general we suggest that this requirement and that of low elastic stiffness are best explained by plastic failure of the country rocks during intrusion growth, in agreement with field observations.

A final consideration in modelling the emplacement of laccoliths and sills is the likelihood that they grow by vertical stacking of multiple pulses. For the intrusions assessed here we find that intrusion of thin pulses alleviates the requirement for low stiffness country rocks as well as bringing down the fracture toughness to more acceptable values. However, in all cases an effective emplacement depth that is lower than the true depth is required. Nevertheless, construction of laccoliths and sills by multiple pulses together with plastic failure of host rocks during emplacement appears to reconcile the mismatch between observations and theory. It should be noted that both of these effects have yet to be implemented in numerical models, and that although growth of laccoliths by multiple pulses is widely accepted, the incremental emplacement of sills is still debated.

The origin of the bifurcation in the data set between laccoliths and large mafic sills (Fig. 9) is an outstanding problem for future research. However, since laccoliths and large mafic sills share common evolutionary pathways, we argue that the bifurcation is not related to differences in emplacement depth or composition, density or viscosity. Instead, we suggest that whether an

intrusion ends up in the laccolith or large mafic sill field depends largely on a combination of magma productivity and the rates of magma supply and solidification. Hence, low melt production regimes will be only capable of delivering a sufficient volume of magma to form a laccolith at low $G$. By comparison high melt productivity regimes will ensure enough magma supply to allow lengthening to large $G$, aided by the additional effect of the magma weight. Magma supply rate will also be a contributing factor in both scenarios, as this will influence how long flow in the growing intrusion can continue before solidification occurs. This latter effect might also provide an alternative explanation for the $a < 0.5$ scaling of large mafic sills, although this requires further development of both numerical and laboratory modelling of sill emplacement incorporating the effects of solidification (e.g., using the approach of Lister 1995 and Bolchover and Lister 1999).

When $L \sim 8\text{–}12$ km there is a transition between laccoliths and plutons and layered mafic intrusions, which are characterised by a scaling regime with $a < 1$. This transition corresponds to a change in emplacement mechanism from one dominated by roof lifting to one dominated by floor depression. As such, it represents a "lifting limit" (Fig. 9), which is likely controlled by the tendency for plutons and layered intrusions to be emplaced at deeper crustal levels than laccoliths. The origin of the $a < 1$ scaling for plutons and layered mafic intrusions, as well as the tendency for $a$ to decrease with $L$ remain poorly understood. We note that growth of these types of intrusions, together with composite batholiths, is likely governed by the mass balance of magma transfer from the source to the emplacement site, and how this transfer and space for growth is accommodated by large-scale deformation of the crust. Growth of plutons and layered intrusions by vertical stacking of pulses is expected to be an important contributing factor in both of these processes. A significant challenge for future research will be to couple these constraints, as well as heat transfer and solidification within a self-consistent model of intrusion growth in the mid- to lower crust.

Lastly, we have given some consideration to timescales of emplacement, which in general will increase with increasing intrusion size and volume (Fig. 9). Assuming reasonable estimates for magma volumetric flow rate, laccoliths and sills can be emplaced in 10's of years to k-years, while single pulses can potentially be injected over months to a few years. These results are consistent with thermal modelling studies and rare, direct observation of shallow intrusion growth from surface deformation. Timescales for larger laccoliths, plutons and layered mafic intrusions are likely to be strongly influenced by the time lag between rapidly emplaced pulses, which in turn relates to the productivity and magma supply rate in the source. Hence plutons and layered mafic intrusions grow over ka to Ma timescales, in agreement with constraints from precise geochronology.

# References

Abdelmalak MM, Mourgues R, Galland O, Bureau D (2012) Fracture mode analysis and related surface deformation during dyke intrusion Results from 2D experimental modelling. Earth Planet Sci Lett 359–360:93–105

Annen C (2011) Implications of incremental emplacement of magma bodies for magma differentiation, thermal aureole dimensions and plutonism–volcanism relationships. Tectonophysics 500:3–10

Babiker M, Gudmundsson A (2004) Geometry, structure and emplacement of mafic dykes in the Red Sea Hills, Sudan. J Afr Earth Sc 38:279–292

Barnes SJ, Cruden A, Arnt N, Saumur B (2016) The mineral system approach applied to magmatic Ni-Cu-PGE sulfide deposits. Ore Geol Rev 76:296–316

Bédard JH, Naslund HR, Nabelek P, Winpenny A, Hryciuk M, Hayes B, Steigerwaldt K, Hadlari T, Rainbird R, Dewing K, Girard E (2012) Fault-mediated melt ascent in a Neoproterozoic continental flood basalt province, the Franklin sills, Victoria Island, Canada. Geol Soc Am Bull 124:723–736

Bolchover P, Lister JR (1999) The effect of solidification on fluid-driven fracture, with application to bladed dykes. Proc R Soc A 455:2389–2409

Bunger AP, Cruden AR (2011a) Modeling the growth of laccoliths and large mafic sills: the role of magma body forces. J Geophys Res 116:B02203. doi:10.1029/2010JB007648

Bunger A, Cruden A (2011b) Correction to "Modelling the growth of laccoliths and large mafic sills: the role of magma body forces". J Geophys Res 116:B08211. doi:10.1029/2011JB008618

Bunger A, Menand T, Cruden A, Zhang X, Halls H (2013) Analytical predictions for a natural spacing within dyke swarms. Earth Planet Sci Lett 375:270–279

Bradley J (1965) Intrusion of major dolerite sills. Trans R Soc 3:27–55

Brown EH, McClelland WC (2000) Pluton emplacement by sheeting and vertical ballooning in part of the southeast Coast Plutonic Complex, British Columbia. Geol Soc Am Bull 112:708–719

Cawthorn RG (ed) (1996) Layered intrusions. Elsevier Science, Amsterdam, p 531

Clough CT, Maufe HB, Bailey EB (1909) The cauldron-subsidence of Glen Coe, and the associated igneous phenomena. J Geol Soc London 65:611–678

Coleman D, Gray W, Glazner AF (2004) Rethinking the emplacement and evolution of zoned plutons: geochronologic evidence for incremental assembly of the Tuolumne Intrusive Suite, California. Geology 32:433–436

Corazzato C, Groppelli G (2004) Depth, geometry and emplacement of sills to laccoliths and their host-rock relationships: Montecampione group, Southern Alps, Italy. Geol Soc London Spec Publ 234:175–200

Corry CE (1988) Laccoliths: mechanics of emplacement and growth. Geol Soc Am 220:110 (Special Publication)

Cruden AR (1998) On the emplacement of tabular granites. J Geol Soc London 155:853–862

Cruden AR (2006) Emplacement and growth of plutons: implications for rates of melting and mass transfer in continental crust. In: Brown M, Rushmer T (eds) Evolution and differentiation of the continental crust. Cambridge University Press, Cambridge, pp 455–519

Cruden AR (2008) Oskarshamn site investigation: emplacement mechanisms and structural influence of a younger granite intrusion into older wall rocks—a principal study with application to the Götemar and Uthammar granites. SKB. Swedish Nuclear Fuel and Waste Management Co., R-Report R-08-138, 48 p

Cruden AR, McCaffrey KJW (2001) Growth of plutons by floor subsidence: implications for rates of emplacement, intrusion spacing and melt-extraction mechanisms. Phys Chem Earth Part A 26:303–315

Cruden AR, Mazzarini F, Bunger A, Musemeci G (2009) Geometry, scaling relationships and emplacement dynamics of a ca. 6 Ma shallow felsic sill complex, Calamita Peninsula, Elba Island, Italy. Eos

Trans AGU, 90(52), Fall Meeting Supplement, Abstract T13A-1843

Daly RA (1905) The classification of igneous intrusive bodies. J Geol 13:485–508

Delaney PT, Pollard DD (1981) Deformation of host rocks and flow of magma during growth of minette dikes and breccia-bearing intrusions near Ship Rock, New Mexico. US Geological Survey Professional Paper 1201

Detournay E (2004) Propagation regimes of fluid-driven fractures in impermeable rocks. Int J Geomech 4:35–45. doi:10.1061/(ASCE)1532-3641(2004)4:1(35)

Dixon JM, Simpson DG (1987) Centrifuge modelling of laccolith intrusion. J Struct Geol 9(87–103):1987

Ernst RE, Buchan KL, Campbell IH (2005) Frontiers in large igneous province research. Lithos 79:271–297

Francis EH (1982) Magma and sediment—I. Emplacement mechanism of late Carboniferous tholeiite sills in northern Britain. J Geol Soc London 139:1–20

Friese N, Vollbrecht A, Tanner DC, Fahlbusch W, Weidemann M (2012) Multi-stage emplacement of the Götemar Pluton, SE Sweden: new evidence inferred from field observations and microfabric analysis, including cathodoluminescence microscopy. Int J Earth Sci 101:1149–1167

Galland this volume

Galland O, Scheibert J (2013) Analytical model of surface uplift above axisymmetric flat-lying magma intrusions: implications for sill emplacement and geodesy. J Volcanol Geoth Res 253:114–130

Galland O, Cobbold PR, Hallot E, de Bremond d'Ars, Delavaud G (2006) Use of vegetable oil and silica powder for scale modeling of magmatic intrusion in a deforming brittle crust. Earth Planet Sci Lett 243:786–804

Galland O, Planke S, Neumann E-R, Malthe-Sørenssen A (2009) Experimental modelling of shallow magma emplacement: application to saucer-shaped intrusions. Earth Planet Sci Lett 277:373–383

Geshi N, Kusumoto S, Gudmundsson A (2010) Geometric difference between non-feeder and feeder dikes. Geology 38:195–198

Gilbert GK (1877) Report on the Geology of the Henry Mountains. U.S. Geographical and Geological Survey of the Rocky Mountain Region, Government Printing Office, Washington, 160 p

Glazner AF, Bartley JM, Coleman DS, Gray W, Taylor RZ (2004) Are plutons assembled over millions of years by amalgamation from small magma chambers? GSA Today 14:4–11

Gudmundsson A (2011a) Rock fractures in geological processes. Cambridge University Press, Cambridge, 592 p

Gudmundsson this volume

Gudmundsson A (2011b) Deflection of dykes into sills at discontinuities and magma-chamber formation. Tectonophysics 500:50–64

Grocott J, Arevalo C, Welkner D, Cruden AR (2009) Fault-assisted vertical pluton growth: Coastal Cordillera, northern Chilean Andes. J Geol Soc London 166:295–301

Halls HC, Fahrig WF (eds) (1987) Mafic Dyke swarms. Geological Association of Canada, Special Paper 34

Hamilton WB (1965) Diabase sheets of the Taylor Glacier Region, Victoria Land, Antarctica. US Geological Survey, Professional Papers 456-B, 77 p

Hansen DM, Cartwright J (2006) The three-dimensional geometry and growth of forced folds above saucer-shaped igneous sills. J Struct Geol 28:1520–1535

Hergt JM, Brauns CM (2001) On the origin of Tasmanian dolerites. Aust J Earth Sci 48:543–549

Horsman E, Morgan S, de Saint Blanquat M, Habert G, Nugent A, Hunter RA, Tikoff B (2010) Emplacement and assembly of shallow intrusions from multiple magma pulses, Henry Mountains, Utah. Earth Environ Sci Trans R Soc Edinburgh 100:1–16

Hunt CB, Averitt P, Miller RL (1953) Geology and geography of the Henry Mountains region, Utah. U.S. Geological survey professional paper 228, 234 p

Hutton DHW (2009) Insights into magmatism in volcanic margins: bridge structures and a new mechanism of basic sill emplacement—Theron Mountains, Antarctica. Petrol Geosci 15:269–278

Jackson MD, Pollard DD (1988) The laccolith-stock controversy: new results from the southern Henry Mountains, Utah. Geol Soc Am Bull 100:117–139

Johnson AM, Pollard DD (1973) Mechanics of growth of some laccolithic intrusions in the Henry Mountains, Utah, I. Field observations, Gilbert's model, physical properties and flow of the magma. Tectonophysics 18:261–309

Kavanagh JL, Menand T, Sparks RSJ (2006) An experimental investigation of sill formation and propagation in layered elastic media. Earth Planet Sci Lett 245:799–813

Kavanagh J, Boutelier D, Cruden A (2015) The mechanics of sill inception, propagation and growth: experimental evidence for rapid reduction in magmatic overpressure. Earth Planet Sci Lett 421:117–128

Klimczak C, Schultz RA, Parashar R, Reeves DM (2010) Cubic law with aperture-length correlation: implications for network scale fluid flow. Hydrogeol J 18:851–862

Koch F, Johnson A, Pollard DD (1981) Monoclinal bending of strata over laccolithic intrusions. Tectonophysics 74:T21–T31

Leaman DE (1975) Form, mechanism, and control of dolerite intrusion near Hobart, Tasmania. Aust J Earth Sci 22:175–186

Lister JR (1995) Fluid mechanical models of the interaction between solidification and flow in dykes. In: Physics and chemistry of Dykes, Balkema, pp 115–124

Leuthold J, Muntener O, Baumgartner LP, Putlitz B, Ovtcharova M, Schaltegger U (2012) Time resolved construction of a bimodal laccolith (Torres del Paine, Patagonia). Earth Planet Sci Lett 325–326:85–92

Magee C, Muirhead JD, Karvelas A, Holford SP, Jackson CAL, Bastow ID, Schofield N, Stevenson CTE, McLean C, McCarthy W, Shtukert O (2016) Lateral magma flow in mafic sill complexes. Geosphere 12:809. doi:10.1130/GES01256.1

Malthe-Sørenssen A, Planke S, Svensen H, Jamtveit B (2004) Formation of saucer-shaped sills. In: Physical geology of high-level magmatic systems, vol 234. Geological Society, London, Special Publications, pp 215–227

Marsh BD (2004) A magmatic mush column Rosetta Stone: the McMurdo Dry Valleys of Antarctica. EOS, Trans Am Geophys Union 85:497–508

Mathieu L, van Wyk de Vries B, Holohan EP, Troll VR (2008) Dykes, cups, saucers and sills: analogue experiments on magma intrusion into brittle rocks. Earth Planet Sci Lett 271:1–13

McCaffrey K, Petford N (1997) Are granitic plutons scale invariant? J Geol Soc London 154:1–14

McQuarrie N, Rogers DW (1998) Subsidence of a volcanic basin by flexure and lower crustal flow: the eastern Snake River Palin, Idaho. Tectonics 17:203–220

Miles AJ, Cartwright JA (2010) Hybrid flow sills: a new mode of igneous sheet intrusion. Geology 38:343–346

Miller JS, Matzel JEP, Miller CF, Burgess SD, Miller RB (2007) Zircon growth and recycling during the assembly of large, composite arc plutons. J Volcanol Geotherm Res 167:282–299

Menand T (2008) The mechanics and dynamics of sills in layered elastic rocks and their implications for the growth of laccoliths and other igneous complexes. Earth Planet Sci Lett 267:93–99. doi:10.1016/j.epsl.2007.11.043

Menand T (2011) Physical controls and depth of emplacement of igneous bodies: a review. Tectonophysics 500:11–19

Menand T, de Saint Blanquat M, Annen C (2011) Emplacement of magma pulses and growth of magma bodies. Tectonophysics 500:1–2

Menand T, Annen C, de Saint Blanquat M (2015) Rates of magma transfer in the crust: Insights into magma reservoir recharge and pluton growth. Geology 43:199–202

Michel J, Baumgartner L, Putlitz B, Schaltegger U, Ovtcharova M (2008) Incremental growth of the Patagonian Torres del Paine laccolith over 90 ky. Geology 36:459–465

Mudge MR (1968) Depth control of some concordant intrusions. Geol Soc Am Bull 79:315–332

Muirhead JD, Airoldi G, Rowland JV, White JDL (2012) Interconnected sills and inclined sheet intrusions controlshallow magma transport in the Ferrar large igneous province, Antarctica. Geol Soc Am Bull 124:162–180

Myers JS (1975) Cauldron subsidence and fluidization: mechanisms of intrusion of the Coastal Batholith of Peru into its own volcanic ejecta. Geol Soc Am Bull 86:1209–1220

Nicholson R, Pollard D (1985) Dilation and linkage of echelon cracks. J Struct Geol 7:583–590

Olson JE (2003) Sublinear scaling of fracture aperture versus length: An exception or the rule? J Geophys Res 108:2413. doi:10.1029/2001JB000419, B9

Paterson SR, Fowler TK Jr, Miller RB (1996) Pluton emplacement in arcs: a crustal-scale exchange process. Trans R Soc Edinburgh: Earth Sci 87:115–123

Perkins TK, Kern LR (1961) Widths of hydraulic fractures. J Petrol Technol 13:937–950

Petford N, Cruden AR, McCaffrey KJW, Vigneresse J-L (2000) Dynamics of granitic magma formation, transport and emplacement in the Earth's crust. Nature 408:669–673

Planke et al. this volume

Pollard DD, Johnson AM (1973) Mechanisms of some laccolithic intrusions in the Henry Mountains, Utah, Part II: bending and failure of overburden and sill formation. Tectonophysics 18:311–354

Polteau S, Mazzini A, Galland O, Planke S, Malthe-Sørenssen A (2008) Saucer-shaped intrusions: Occurrences, emplacement and implications. Earth Planet Sci Lett 266:195–204. doi:10.1016/j.epsl.2007.11.015

Price NJ, Cosgrove JW (1990) Analysis of geological structures. Cambridge University Press, Cambridge, p 507

Puffer JH, Block KA, Steiner JC (2009) Transmission of flood basalts through a shallow crustal sill and the correlation of sill layers with extrusive flows: the Palisades intrusive system and the basalts of the Newark basin, New Jersey, U.S.A. J Geol 117:139–155

Putlitz B, Baumgartner LP, Oberhaensli R, Diamond L, Altenberger U (2001) The Torres del Paine Laccolith (Chile); intrusion and metamorphism. In: XI Goldschmidt Conference, Abstract No. 3534. Hot Springs, United States

Quick JE, Sinigoi S, Mayer A (1994) Emplacement dynamics of a large mafic intrusion in the lower crust, Ivrea-Verbano Zone, northern Italy. J Geophys Res 99:21559–21573

Rivalta E, Taisne B, Bunger AP, Katz RF (2015) A review of mechanical models of dike propagation: Schools of thought, results and future directions. Tectonophysics 638:1–42

Rocchi S, Westerman DS, Dini A, Innocenti F, Tonarini S (2002) Two-stage growth of laccoliths at Elba Island, Italy. Geology 30:983–986

Rocchi S, Westerman DS, Dini A, Farina F (2010) Intrusive sheets and sheeted intrusions at Elba Island (Italy). Geosphere 6:225–236

Robertson WA, Baragar WRA (1972) The petrology and paleomagnetism of the Coronation Sills. Can J Earth Sci 9:123–140

Roman-Berdiel T, Gapais D, Brun JP (1995) Analogue models of laccolith formation. J Struct Geol 17:1337–1346

de Saint Blanquat M, Law RD, Bouchez J-L, Morgan SS (2001) Internal structure and emplacement of the Papoose Flat pluton: an integrated structural, petrographic, and magnetic susceptibility study. Geol Soc Am Bull 113:976–995

de Saint Blanquat M, Habert G, Horsman E, Morgan S, Tikoff B, Launeau P, Gleizes G (2006) Mechanisms and duration of non-tectonically assisted magma emplacement in the upper crust: The Black Mesa pluton, Henry Mountains, Utah. Tectonophysics 428:1–31

de Saint Blanquat M, Horsman E, Habert G, Morgan S, Vanderhaeghe O, Law R, Tikoff B (2011) Multiscale magmatic cyclicity, duration of pluton construction, and the paradoxical relationship between tectonism and plutonism in continental arcs. Tectonophysics 500:20–33

Saumur BM, Cruden AR (2016) On the emplacement of the Voisey's Bay intrusion (Labrador, Canada). Geol Soc Am Bull 128:147–168

Savitski AA, Detournay E (2002) Propagation of a penny-shaped fluid-driven fracture in an impermeable rock: asymptotic solutions. Int J Solids Struct 39:6311–6337

Scaillet B, Searle MP (2006) Mechanisms and timescales of felsic magma segregation, ascent and emplacement in the Himalaya. Geol Soc London Spec Publ 268:293–308

Schaltegger U, Brack P, Ovtcharova M, Peytcheva I, Schoene B, Stracke A, Marocchi M, Bargossi GM (2009) Zircon and titanite recording 1.5 million years of magma accretion, crystallization and initial cooling in a composite pluton (southern Adamello batholith, northern Italy). Earth Planet Sci Lett 286:208–218

Schultz RA, Soliva R, Fossen H, Okubo CH (2008a) Dependence of displacement–length scaling relations for fractures and deformation bands on the volumetric changes across them. J Struct Geol 30:1405–1411

Schultz RA, Mege D, Diot H (2008b) Emplacement conditions of igneous dikes in Ethiopian Traps. J Volcanol Geotherm Res 178:683–692

Schofield NJ, Brown DJ, Magee C, Stevenson CT (2012) Sill morphology and comparison of brittle and non-brittle emplacement mechanisms. J Geol Soc London 169:127–141

Shirley DN (1987) Differentiation and compaction in the Palisades Sill, New Jersey. J Petrol 28:835–865

Skarmeta JJ, Castelli JC (1997) Intrusion sintectonica del granito de las Torres del Paine, Andes Patagonicos de Chile. Rev Geol Chile 24:55–74

Smith RJ (2009) Use and misuse of the reduced major axis for line-fitting. Am J Phys Anthropol 140:476–486

Sneddon IN, Lowengrub M (1969) Crack problems in the classical theory of elasticity. Wiley, New York, p 230

Thomson K (2007) Determining magma flow in sills, dykes and laccoliths and their implications for sill emplacement mechanisms. Bull Volc 70:183–201

Thomson K, Hutton D (2004) Geometry and growth of sill complexes: insights using 3D seismic from the North Rockall Trough. Bull Volc 66:364–375

Thomson K, Schofield N (2008) Lithological and structural controls on the emplacement and morphology of sills in sedimentary basins. Geol Soc London Spec Publ 302:31–44

Vigneresse JL (1995) Control of granite emplacement by regional deformation. Tectonophysics 249:173–186

Walker GPL (1993) Re-evaluation of inclined intrusive sheets and dykes in the Cuillins volcano, Isle of Skye. Geol Soc London Spec Publ 76:489–497

Walker KR (1969) The Palisades sill, New Jersey: a reinvestigation. Geological Society of America Special Paper 111, 155 p

Walker RJ (2016) Controls on transgressive sill growth. Geology 44:99–102

White SM, Crisp JA, Spera FJ (2006) Long-term volumetric eruption rates and magma budgets. Geochem Geophys Geosyst 7:Q03010. doi:10.1029/2005GC001002

Westerman et al. this volume

Wiebe RA, Collins WJ (1998) Depositional features and stratigraphic sections in granitic plutons: Implications for the emplacement and crystallization of granitic magma. J Struct Geol 20:1273–1289

Wilson PIR, McCaffrey KJW, Wilson R, Jarvis I, Holdsworth RE (2016) Deformation structures associated with the Trachyte Mesa intrusion, Henry Mountains, Utah: implications for sill and laccolith emplacement mechanisms. J Struct Geol 87:30–46

Zenzri H, Kerr LM (2001) Mechanical analyses of the emplacement of laccoliths and lopoliths. J Geophys Res 106:13781–13792